

Dear editor,

Thanks for your careful reading and the suggestion of the detailed corrections for improving our manuscript. We corrected accordingly and all revisions were labelled in red in the following differ version.

Line 273, 308, 331 and 333, replace “transportation” with transport

Corrected accordingly.

Line 320, replace “others” with “other factors.”

Corrected accordingly.

Line 333, replace “contrition” with “contribution”

Corrected accordingly.

Line 335, replace “accompanied” with “also observed”

Corrected accordingly.

Line 457, replace “the amount quantification uncertainty” with “an uncertainty”

Corrected accordingly.

Line 446, 472 and 810, replaced “initialed” with either “initialized” or “derived”

Corrected accordingly.

1 Efficient N₂O₅ Uptake and NO₃ Oxidation in the Outflow of Urban Beijing

2 Haichao Wang¹, Keding Lu^{1*}, Song Guo¹, Zhijun Wu¹, Dongjie Shang¹, Zhaofeng Tan¹, Yujue Wang¹,
3 Michael Le Breton², Shengrong Lou³, Mingjin Tang⁴, Yusheng Wu¹, Jing Zheng¹, Limin Zeng¹,
4 Mattias Hallquist², Min Hu¹ and Yuanhang Zhang^{1, 5}

5

6 ¹State Key Joint Laboratory of Environmental Simulation and Pollution Control, College of
7 Environmental Sciences and Engineering, Peking University, Beijing, China.

8 ²Department of Chemistry and Molecular Biology, University of Gothenburg, Gothenburg, Sweden

9 ³Shanghai Academy of Environmental Sciences, Shanghai, China

10 ⁴State Key Laboratory of Organic Geochemistry and Guangdong Key Laboratory of Environmental
11 Protection and Resources Utilization, Guangzhou Institute of Geochemistry, Chinese Academy of
12 Sciences, Guangzhou, China

13 ⁵CAS Center for Excellence in Regional Atmospheric Environment, Chinese Academy of Sciences,
14 Xiamen, China

15

16 *Corresponding to: Keding Lu (k.lu@pku.edu.cn)

17

18 **Abstract.** Nocturnal reactive nitrogen compounds play an important role in regional air pollution. Here
19 we present the measurements of dinitrogen pentoxide (N₂O₅) associated with nitryl chloride (ClNO₂)
20 and particulate nitrate (pNO₃⁻) in a suburban site of Beijing in the summer of 2016. High levels of
21 N₂O₅ and ClNO₂ were observed in the outflow of the urban Beijing air masses, with 1-min average
22 maxima of 937 pptv and 2900 pptv, respectively. The N₂O₅ uptake coefficients, γ , and ClNO₂ yield, f ,
23 were experimentally determined from the observed parameters. The N₂O₅ uptake coefficient ranged
24 from 0.012 to 0.055, with an average of 0.034 ± 0.018 , which is in the upper range of previous field
25 studies reported in North America and Europe but is a moderate value in the North China Plain (NCP),
26 which reflects efficient N₂O₅ heterogeneous processes in Beijing. The ClNO₂ yield exhibited high
27 variability, with a range of 0.50 to unity and an average of 0.73 ± 0.25 . The concentration of the nitrate
28 radical (NO₃) was calculated assuming that the thermal equilibrium between NO₃ and N₂O₅ was
29 maintained. In NO_x-rich air masses, the oxidation of nocturnal biogenic volatile organic compounds
30 (BVOCs) was dominated by NO₃ rather than O₃. The production rate of organic nitrate (ON) via
31 NO₃+BVOCs was significant, with an average of 0.10 ± 0.07 ppbv h⁻¹. We highlight the importance
32 of NO₃ oxidation of VOCs in the formation of ON and subsequent secondary organic aerosols in
33 summer in Beijing.

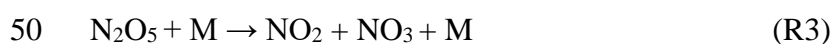
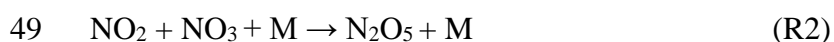
34

35

36

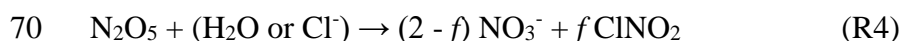
37 1. Introduction

38 It has been well recognized that reactive nitrogen compounds, specifically the nitrate radical (NO₃)
39 and dinitrogen pentoxide (N₂O₅), play a key role in nighttime chemistry (Wayne et al., 1991; Brown
40 and Stutz, 2012). NO₃ is the most important oxidant in the nighttime and can be considered the
41 nighttime analogue of the hydroxyl radical (OH) for certain VOCs (Wayne et al., 1991; Benton et al.,
42 2010). NO₃ can initiate the removal of many kind of anthropogenic and biogenic emissions after sunset.
43 In NO_x-rich plumes, NO₃ is responsible for the vast majority of the oxidation of biogenic VOCs
44 because of its rapid reactions with unsaturated hydrocarbons (Edwards et al., 2017). NO₃ is
45 predominantly formed by the reaction of NO₂ with O₃ (R1) and further reacts with NO₂ to produce
46 N₂O₅ (R2). N₂O₅ is rapidly decomposed back to NO₃ (R3), NO₃ and N₂O₅ are in dynamic equilibrium
47 in the troposphere.



51 Photolysis of NO₃ and the reaction of NO₃ with NO are rapid, which lead to a daytime NO₃ lifetime
52 being shorter than 5 s with extremely low concentrations, whereas in low-NO air masses, the fate of
53 NO₃ is mainly controlled by the mixing ratios of various VOCs and N₂O₅ heterogeneous hydrolysis
54 because the two terms are the dominating loss pathways of NO₃ and N₂O₅. The VOCs reaction is
55 significant downwind of an urban area or a strongly urban-influenced forested area in summer. The
56 NO₃ oxidation of VOCs was responsible for more than 70% nocturnal NO₃ loss in Houston (Stutz et
57 al., 2010) and contributed approximately 50% in the forest region in Germany (Geyer et al., 2001).
58 The reactions of NO₃ with several BVOCs produce considerable amounts of organic nitrates (ON)
59 with efficient yields, which act as important precursors of secondary organic aerosols (SOA). The
60 reaction of NO₃ with isoprene has a SOA mass yield of 23.8% (Ng et al., 2008). For the reaction with
61 monoterpene, such as limonene, the SOA mass yield can reach 174% at ambient temperatures (Boyd
62 et al., 2017). The reactions of NO₃+BVOCs are critical to the studies of aerosols on regional and global
63 scales (Fry et al., 2009; Rollins et al., 2009; Pye et al., 2010; Ng et al., 2017). For example, ON had
64 extensive percentages of fine particulate nitrate (pNO₃⁻) (34% - 44%) in Europe (Kiendler-Scharr et
65 al., 2016).

66 The heterogeneous hydrolysis of N₂O₅ produces soluble nitrate (HNO₃ or NO₃⁻) and nitryl chloride
67 (ClNO₂) on chloride-containing aerosols (R4) (Finlayson-Pitts et al., 1989). This reaction is known to
68 be an important intermediate in the NO_x removal processes (Brown et al., 2006). The pseudo-first order
69 loss rate constant of N₂O₅ via heterogeneous uptake is given in Eq. 1 (Wahner et al., 1998).



$$71 k_{\text{N}_2\text{O}_5} = 0.25 \cdot c \cdot \gamma(\text{N}_2\text{O}_5) \cdot S_a \quad (\text{Eq. 1})$$

72 Where c is the mean molecule speed of N₂O₅, S_a is the aerosol surface concentration and $\gamma(\text{N}_2\text{O}_5)$ is
73 the N₂O₅ uptake coefficient. N₂O₅ heterogeneous hydrolysis is one of the major uncertainties of the
74 NO₃ budget since the N₂O₅ uptake coefficient can be highly variable and difficult to quantify (Brown
75 and Stutz, 2012; Chang et al., 2011; H. C. Wang et al., 2016). Laboratory and field measurement studies

76 have reported that the N_2O_5 uptake coefficient has large variability and ranges from <0.001 to 0.1 ; the
77 N_2O_5 uptake coefficient depends on relative humidity (RH), particle morphology, compositions (water
78 content, nitrate, sulfate, organic or mineral particles) and other factors (Wahner et al., 1998; Mentel et
79 al., 1999; Hallquist et al., 2003; Thornton et al., 2003; Thornton et al., 2005; Brown et al., 2006;
80 Bertram and Thornton, 2009; Tang et al., 2012, 2014; Gaston et al., 2014; Grzanic et al., 2015; Tang et
81 al., 2017). The coupled chemical mechanisms in ambient conditions are still not well understood.
82 ClNO_2 forms and accumulates with a negligible sink during the night and further photolyzes and
83 liberates the chlorine radical (Cl) and NO_2 after sunrise. Hundreds of pptv to ppbv of ClNO_2 can lead
84 to several ppbv of O_3 enhancement and significant primary RO_x production (Osthoff et al., 2008;
85 Thornton et al., 2010; McLaren et al., 2010; Riedel et al., 2014; Sarwar et al., 2014; Tham et al., 2016).

86 Large amounts of NO_x have been emitted for the past several decades in China, but comprehensive
87 field studies of the nighttime chemical processes of reactive nitrogen oxides remain sparse. Previous
88 studies have found high mixing ratios of NO_3 associated with high NO_3 reactivity in the megacities in
89 China, including Shanghai, the Pearl River Delta (PRD) and Beijing (Li et al., 2012; Wang et al., 2013;
90 Wang et al., 2015). The N_2O_5 concentration was elevated in Beijing (H. C. Wang et al., 2017a; H. C.
91 Wang et al., 2017c) but was moderate in other places of North China Plain (NCP), such as Wangdu,
92 Jinan and Mount Tai (Tham et al., 2016; X. F. Wang et al., 2017; Z. Wang et al., 2017). Recently, the
93 N_2O_5 uptake coefficients were determined to be very high, even up to 0.1 in NCP, but the reason is still
94 not well studied (H. C. Wang et al., 2017c; X. F. Wang et al., 2017; Z. Wang et al., 2017). Reactive
95 N_2O_5 chemistry was also reported in Hong Kong, and showed the highest field-observed N_2O_5
96 concentration to date (T. Wang et al., 2016; Brown et al., 2016). Observations and model simulations
97 revealed that fast heterogeneous uptake of N_2O_5 is an important pathway of pNO_3^- formation in China
98 (H. C. Wang et al., 2017b; H. C. Wang et al., 2017c; Z. Wang et al., 2017; Su et al., 2017); the reaction
99 also contributed significantly to removal (Z. Wang et al., 2017; Brown et al., 2016). Moreover, chlorine
100 activation from N_2O_5 uptake had a significant effect on daytime photolysis chemistry in China (Xue et
101 al., 2015; Li et al., 2016; Tham et al., 2016; T. Wang et al., 2016).

102 In this study, to quantify the contribution of NO_3 and N_2O_5 chemistry to the atmospheric oxidation
103 capacity and the NO_x removal process in the outflow of urban Beijing, we report the measurement of
104 N_2O_5 , ClNO_2 , and related species in the surface layer of a suburban site in Beijing and determine the
105 N_2O_5 heterogeneous uptake coefficients and ClNO_2 yields. The nighttime NO_3 oxidation of biogenic
106 VOCs and its impact on the ON formation in the NO_x -rich region were diagnosed. Finally, the
107 nighttime NO_x removal via NO_3 and N_2O_5 chemistry was estimated and discussed.

108 **2. Method**

109 **2.1 The site**

110 Within the framework of a Sino-Sweden joint research project, “Photochemical Smog in China”, a
111 summer field campaign was conducted in Beijing to enhance our understanding of the secondary
112 chemistry via photochemical smog and the heterogeneous reactions (Hallquist et al., 2016). The data
113 presented here were collected at a regional site, PKU-CP (Peking University Changping campus), from
114 23 May to 5 June 2016. The measurement site is located in the northern rural area of Beijing,
115 approximately 45 km from the city center; the closest road is approximately 1 km to the south, and
116 there are no major industry in the surroundings (Figure. 1). The site is surrounded to the north, east

117 and west by mountains. The general feature of this site is that it captures air masses with strong
118 influences from both urban and biogenic emissions. Instruments were set up on the fifth floor of the
119 main building of the campus with inlets approximately 12 m above the ground. Time is given in this
120 paper as CNST (Chinese National Standard Time = UTC+8 h). During the campaign, sunrise was at
121 05:00 CNST and sunset was at 19:30 CNST.

122 **2.2 Instrument setup**

123 A comprehensive suite of trace gas compounds and aerosol properties was measured in the field study,
124 and the details are listed in Table 1. N_2O_5 was measured by a newly developed cavity enhanced
125 absorption spectrometer (CEAS; H. C. Wang et al., 2017a). In the CEAS, ambient N_2O_5 was thermally
126 decomposed to NO_3 in a perfluoroalkoxy alkanes (PFA) tube (length: 35 cm, I.D.: 4.35 mm) heated to
127 120 °C and was then detected within a PFA resonator cavity; the cavity was heated to 80 °C to prevent
128 NO_3 reacting back to N_2O_5 . Ambient gas was sampled with a 1.5-m sampling line (I.D.: 4.35 mm) with
129 a flow rate of 2.0 L min^{-1} . NO was injected for 20 seconds to destroy NO_3 from N_2O_5 thermal
130 decomposition in a 5-minute cycle, and the corresponding measurements were then used as reference
131 spectra. A Teflon polytetrafluoroethylene (PTFE) filter was used in the front of the sampling module
132 to remove ambient aerosol particles. The filter was replaced with a fresh one every hour to avoid the
133 decrease of N_2O_5 transmission efficiency due to aerosol accumulation on the filter. The limit of
134 detection (LOD) was 2.7 pptv (1σ), and the measurement uncertainty was 19%.

135 ClNO_2 and N_2O_5 were also detected using a Time of Flight Chemical Ionization Mass Spectrometer
136 (ToF-CIMS) with the Filter Inlet for Gas and AEROsols (FIGAERO; Lopez-Hilfiker et al., 2014;
137 Bannan et al., 2015). Briefly, the gas phase species were measured via a 2-m-long, 6-mm-outer-
138 diameter PFA inlet while the particles were simultaneously collected on a Teflon filter via a separate
139 2-m-long, 10-mm-outer-diameter copper tubing inlet; both had flow rates of 2 L min^{-1} . The gas phase
140 was measured for 25 minutes at 1 Hz, and the FIGAERO instrument was then switched to place the
141 filter in front of the ion molecule region; it was then heated incrementally to 200 °C to desorb all the
142 mass from the filter to be measured in the gas phase, which resulted in high-resolution thermograms.
143 Formic acid calibrations were performed daily using a permeation source maintained at 40 °C. Post-
144 campaign laboratory calibrations of N_2O_5 were first normalized to the campaign formic acid
145 calibrations to account for any change in sensitivity (Le Breton et al., 2014). Then, ClNO_2
146 measurements were quantified by passing the N_2O_5 over a wetted NaCl bed to produce ClNO_2 . The
147 decrease in N_2O_5 from the reaction with NaCl was assumed to be equal to the concentration of ClNO_2
148 produced (i.e., 100% yield). The sensitivities of the CIMS to N_2O_5 and ClNO_2 were found to be 9.5
149 and 1.2 ion counts per pptv Hz^{-1} , respectively, with errors of 23% and 25% for ClNO_2 and N_2O_5 ,
150 respectively. The LOD for ClNO_2 and N_2O_5 were 16 and 8 pptv, respectively. An intercomparison of
151 N_2O_5 measurements between the CEAS and FIGAERO-ToF-CIMS showed good agreement; a
152 companion paper on chlorine photochemical activation during this campaign gives detailed
153 intercomparison results of N_2O_5 measured by the two different techniques (Le Breton et al., 2018).

154 Sub-micron aerosol composition ($\text{PM}_{1.0}$), including nitrate, sulfate, chloride, ammonium and
155 organic compounds, were measured by a High Resolution Time of Flight Aerosol Mass Spectrometer
156 (HR-ToF-AMS) (De Carlo et al, 2006, Zheng et al., 2017). Particle number and size distribution
157 (PNSD) was measured by a scanning mobility particle sizer (SMPS, TSI 3936) and an aerosol particle

158 sizer (APS, TSI 3321) (Yue et al., 2009). SMPS measured the particles in the range between 3.5 nm
159 and 523.3 nm in diameter, and APS measured the particles with a diameter range from 597.6 nm to
160 10.0 μm . S_a was calculated based on the dry-state particle number and geometric diameter in each size
161 bin (3.5 nm - 2.5 μm). Dry-state S_a was corrected to wet particle-state S_a for particle hygroscopicity by
162 a growth factor. The growth factor, $f(\text{RH})=1 + 8.77 \times (\text{RH}/100)^{9.74}$, was derived from the measurement
163 of aerosol extinction as a function of RH in autumn in Beijing and is valid for $30\% < \text{RH} < 90\%$ (Liu
164 et al., 2013). The uncertainty of the wet aerosol surface areas was estimated to be $\sim 30\%$, associated
165 from the error from dry PNSD measurement ($\sim 20\%$) and the growth factor ($\sim 20\%$). During this
166 measurement, fine particles below 500 nm contributed to more than 90% of the total S_a .

167 VOCs were measured by Proton Transfer Reaction Mass Spectrometry (PTR-MS) with a time
168 resolution of 5 minutes (de Gouw and Warneke et al., 2007; Wang et al., 2014). A commercial
169 instrument (Thermo Electron model 42i) equipped with a molybdenum-catalytic converter was used
170 to monitor NO_x . The LODs were 60 pptv (1 min) for NO and 300 pptv (1 min) for NO_2 , with both at a
171 20% precision (Tan et al., 2017). The molybdenum-catalytic technique not only converts NO_2 to NO
172 but also converts ambient NO_y such as peroxyacetyl nitrate (PAN) and HNO_3 . Therefore, the measured
173 NO_2 concentration corresponded to $\text{NO}_2 + \text{NO}_y$ and was normally higher than the real concentration,
174 especially in an aged air mass with high NO_x conditions. In this study, we used a factor of 0.6 to correct
175 the nighttime NO_2 concentration (a detailed explanation is in the Support Information Text S1 and
176 Figure S1). The correction factor (0.6) is the average of the correction factors during nighttime. The
177 standard deviation of the daytime correction factor for all the air masses experienced at Changping site
178 was determined to be 0.27 (1σ). If this uncertainty is extended to the nighttime correction factor, the
179 resulting uncertainty of the nighttime correction is 45%. The uncertainty of NO_2 is 50% when further
180 included the associated measurement uncertainty from calibrations. O_3 was measured by a commercial
181 instrument using ultraviolet (UV) absorption (Thermo Electron model 49i); the LOD was 0.5 ppbv,
182 with an uncertainty of 5%. The mass concentration of $\text{PM}_{2.5}$ was measured using a standard Tapered
183 Element Oscillating Microbalance (TEOM, 1400A analyzer). Meteorological parameters included
184 relative humidity, temperature, pressure, wind speed, and wind direction and were available during the
185 campaign. Photolysis frequencies were calculated from the spectral actinic photon flux density
186 measured by a spectroradiometer (Bohn et al., 2008).

187 **3. Results**

188 **3.1 Overview**

189 During the campaign, the meteorological conditions of the site was high temperature and low relative
190 humidity (RH); the temperature ranged from 10 - 34 $^{\circ}\text{C}$ and was 23 ± 5 $^{\circ}\text{C}$ on average, and RH ranged
191 from 10% - 80%, with an average of $37\% \pm 15\%$. Because of the special terrain of the observation site,
192 the local wind was measured by the in situ meteorological stations; the site has a typical mountain-
193 valley breeze that cannot reflect the general air mass movement patterns at slightly higher altitudes.
194 Figure S2 shows the calculated backward trajectories using the Hybrid Single-Particle Lagrangian
195 Integrated Trajectory (HYSPLIT) model (Draxler and Rolph, 2003). These images show the 24-h
196 backward particle dispersion trajectories for 12:00 local time (CNST) as the starting time during May
197 23 - July 5, 2016. The arrivals of air masses were mainly from the northwest and the south. Therefore,

198 we meteorologically separated the measurement period into two parts. The first three days show that
199 the air masses came from the north or northwest; the air masses represent the background region
200 (defined as Background Air Mass, BAM). The air masses after May 26 originated from the polluted
201 NCP and passed over urban Beijing; they were characterized by large NO_x emissions and severe
202 photochemical pollution (defined as Urban Air Mass, UAM).

203 The time series of N₂O₅, ClNO₂ and other relevant species are shown in Figure 2, and nighttime
204 statistical results are listed in Table S1. The daily 8-h maximum of O₃ concentration exceeded 93 ppbv
205 (Chinese national air quality standard) for 8 of 12 days, and all the O₃-polluted air masses came from
206 the urban region. When the air masses were from the background region, the daily maximum of O₃
207 was only approximately 60 ppbv, much lower than that from the urban region. The NO₂ concentration
208 was elevated, with a nocturnal average value over 10 ppbv during the urban air mass period. The
209 nocturnal nitrate radical production rate, P(NO₃), was large, with an average of 1.2 ± 0.9 ppbv h⁻¹,
210 which is comparable with rates previously reported in the NCP and Hong Kong (Tham et al., 2016;
211 Brown et al., 2016; Z. Wang et al., 2017; X. F. Wang et al., 2017). The daily peaks of N₂O₅ were 100-
212 500 pptv most nights; the maximum of 937 pptv in a 1-min average was observed near 20:00 on the
213 early night of June 2, when the P(NO₃) was up to 4 ppbv h⁻¹. The average mixing ratio of N₂O₅ was 73
214 ± 90 pptv, which is much higher than recent measurements reported in North China (Tham et al., 2016;
215 X. F. Wang et al., 2017; Z. Wang et al., 2017), but much lower than that observed in the residual layer
216 of the outflow from the PRD region, where the N₂O₅ was up to 7.7 ppbv (T. Wang et al., 2016). With
217 an elevated O₃ mixing ratio in the first half of the night, the NO lifetime was only several minutes, and
218 the mixing ratio of NO concentration was observed below the detection limit. During the second half
219 of the night when the O₃ concentration was consumed to low concentration, high levels of NO could
220 occasionally be observed, and N₂O₅ dropped to zero because of the fast titration by NO, such as the
221 events that occurred on the second half of the nights of May 24, 28, 30. The PM_{2.5} mass concentration
222 was moderate during the measurement period, with an average of 26 ± 21 μg m⁻³, and the average S_a
223 was 560 ± 340 μm² cm⁻³. Elevated ClNO₂ was observed with a daily maximum over 800 pptv (1-min
224 average) during the urban air masses period. The maximum of ClNO₂ was observed with 2900 pptv
225 on the morning (05:30) of May 31. The observed ClNO₂ in Beijing was comparable with those reported
226 in NCP (Tham et al., 2016; X. Wang et al., 2017; Z. Wang et al., 2017), but slightly higher than that
227 measured in coastal (e.g., Osthoff et al., 2008) and inland sites (e.g., Thornton et al., 2010). Overall,
228 high ClNO₂ observed in this site suggested fast N₂O₅ heterogeneous hydrolysis and effective ClNO₂
229 yields are common in Beijing.

230 3. 2 Mean diurnal profiles

231 The mean diurnal profiles of the measured NO₂, O₃, N₂O₅, ClNO₂ and the particle chloride content are
232 shown in Figure 3, as well as the calculated NO₃ based on the thermal equilibrium of NO₂, NO₃ and
233 N₂O₅. The left panel show the average results of the BAM period, and the right panels show those of
234 the UAM period. NO₂ and O₃ from the UAM were much higher than those from the BAM, as well as
235 the mixing ratios of N₂O₅, NO₃ and ClNO₂, but the daily variation tendencies of those species in the
236 two kinds of air masses were similar. N₂O₅ began to accumulate in the late afternoon and increased
237 sharply after sunset. A peak occurred near 20:00 and decreased below the instrument detection limit at
238 sunrise. The time that N₂O₅ maxima occurred is similar to our previous observation in urban Beijing

239 (H. C. Wang et al., 2017c). However, the decrease rate of the observed N₂O₅ after the peak time was
 240 much slower than that in urban Beijing, where the N₂O₅ dropped to zero in 2-4 hours, which suggests
 241 a relatively slow N₂O₅ loss rate in suburban Beijing. The daily average peaks of N₂O₅ during the BAM
 242 period and the UAM period were 75 pptv and 150 pptv, respectively. The calculated NO₃ diurnal
 243 profile was quite similar to N₂O₅, and the daily average peaks of NO₃ during the BAM and UAM
 244 periods were approximately 11 pptv and 27 pptv, respectively. The uncertainty of NO₃ calculation was
 245 estimated to be 67% according to Eq. 2, which is dominated by the uncertainty of NO₂ measurement.

$$246 \frac{\Delta[\text{NO}_3]}{[\text{NO}_3]} = \sqrt{\left(\frac{\Delta[\text{N}_2\text{O}_5]}{[\text{N}_2\text{O}_5]}\right)^2 + \left(\frac{\Delta[\text{NO}_2]}{[\text{NO}_2]}\right)^2 + \left(\frac{\Delta[\text{O}_3]}{[\text{O}_3]}\right)^2 + \left(\frac{\Delta K_{\text{eq}}}{K_{\text{eq}}}\right)^2} \quad (\text{Eq. 2})$$

247 The observed ClNO₂ concentrations showed a clear increase after sunset, ClNO₂ reached a
 248 maximum before sunrise for BAM period but around midnight for the UAM period. The diurnal peak
 249 of ClNO₂ in the BAM period was 125 pptv, whereas the diurnal peak of ClNO₂ was over 780 pptv in
 250 the UAM period, and 6 times as high as that in the UAM period. Particulate chloride (Cl⁻) is a key
 251 factor that affects the ClNO₂ yield on aerosol surface. Higher particle chloride leads to higher ClNO₂
 252 yield and promotes the N₂O₅ conversion to ClNO₂ (e.g., Finlayson-Pitts et al., 1989; Behnke et al.,
 253 1997), whereas the particle chloride content during the measurement was below 60 pptv and was much
 254 lower than the mixing ratio of ClNO₂, suggest a nighttime continuously Cl source replenished to
 255 support the ClNO₂ formation. The HYSPLIT showed that the air masses mainly came from continental,
 256 not from the coastal regime, suggested that large amounts of the Cl⁻ were not replenished by NaCl
 257 from marine sources, but possibly replenished by gas-phase HCl through the acid displacement
 258 reaction (Ye et al., 2016). Cl⁻ was found to be correlated strongly with CO and SO₂, likely to originate
 259 from an anthropogenic source, such as power plants or combustion sources (Le Breton et al., 2018).
 260 According to the mass balance, the gas phase HCl for supporting the production of ClNO₂ is several
 261 ppbv per night. The required HCl source indicated the ratio HCl/pCl⁻ is about 10-30, which was found
 262 consistent with the following observation in Beijing. Although the HCl measurement was not available
 263 in this study, note that up to 10 ppbv of HCl was observed in the urban Beijing in September, 2016,
 264 we purpose that the gas phase HCl was sufficient to support the ClNO₂ formation.

265 After sunrise, ClNO₂ was photolyzed and decreased with the increasing photolysis intensity;
 266 However, the ClNO₂ can still survive until noon with the averaged daily maximum of $J(\text{ClNO}_2)$ to be
 267 $1.7 \times 10^{-4} \text{ s}^{-1}$. Similar to the studies reported in London, Texas and Wangdu (Bannan et al., 2015; Faxon
 268 et al., 2015; Tham et al., 2016), we observed sustained elevated ClNO₂ events after sunrise in 5 of 12
 269 days. For example, on the morning of May 30, ClNO₂ increased fast after sunrise and up to 500 pptv
 270 at 8:00 am. Such high ClNO₂ increasing was impossible attribute to the local chemical formation since
 271 N₂O₅ dropped to almost zero and the needed N₂O₅ uptake coefficients were unrealistically high.
 272 Previous study suggested that abundant ClNO₂ produced in the residual layer at night and downward
 273 transportation in the morning may help to explain this phenomenon (Tham et al., 2016).

274 3.3 Variation of N₂O₅ in the background air masses

275 During the BAM period, the O₃ concentration was well in excess of NO₂. In the NO₃ and N₂O₅
276 formation processes, the limited NO₂ in high O₃ region indicates that the variation of NO₂ is more
277 essential to the variation of the N₂O₅ concentration. As shown in Figure 4, during the night of May 24
278 (20:00 - 04:00), the local emission of NO was negligible. O₃ concentration was larger than 25 ppbv,
279 much higher than NO₂ and free of the local NO emission. The N₂O₅ concentration was highly
280 correlated with NO₂ ($R^2 = 0.81$) and the NO₃ production rate ($R^2 = 0.60$), suggests the N₂O₅
281 concentration was solely response to the NO₂ concentration in the background air mass when enough
282 O₃ is presented.

283 3.4 Elevated ClNO₂ to N₂O₅ ratio

284 Large day-to-day variabilities of N₂O₅ and ClNO₂ were observed during the measurement period.
285 Following the work of Osthoff et al. (2008), Mielke et al. (2013), Phillips et al. (2012) and Bannan et
286 al. (2015), we used the concentration ratio of ClNO₂ to N₂O₅, to describe the conversion capacity of
287 N₂O₅ to ClNO₂. Although N₂O₅ is lost to dry deposition in near surface measurements and would drive
288 up the ClNO₂:N₂O₅. The nighttime peak values and mean values of ClNO₂: N₂O₅ were used to calculate
289 the daily ratios (Table S2), the calculation period is from 19:30 to the next day 05:00. The average
290 nighttime ratio ranged from 0.7 to 42.0, with a mean of 7.7 and a median of 6.0. The ClNO₂ formation
291 was effective, with ClNO₂:N₂O₅ ratios larger than 1:1 throughout the campaign, except for the night
292 of May 26, when the ratio was 0.7:1. Previous observations of the ClNO₂:N₂O₅ ratios are summarized
293 in Table 2. Compared with the results conducted in similar continental regions in Europe and America
294 (0.2 - 3.0), the ratios in this work were significantly higher and consistent with the recent studies in
295 the NCP (Tham et al., 2016; X. F. Wang et al., 2017; Z. Wang et al., 2017), which suggests that high
296 ClNO₂: N₂O₅ ratios were ubiquitous in the NCP and implies that the ClNO₂ yield via N₂O₅ uptake is
297 efficient.

298 4. Discussion

299 4.1 Determination of N₂O₅ uptake coefficients

300 A composite term, $\gamma \times f$, was used to evaluate the production of ClNO₂ from N₂O₅ heterogeneous
301 hydrolysis (Mielke et al., 2013). $\gamma \times f$ was estimated by fitting the observed ClNO₂ in a time period
302 when the nighttime concentrations of ClNO₂ increased continuously at night. The increased ClNO₂
303 was assumed to be solely from the N₂O₅ uptake. The fitting was optimized by changing the input of γ
304 $\times f$ associated with the measured N₂O₅ and S_a , until the ClNO₂ increasing was well reproduced (Eq. 3).

$$305 \quad [\text{ClNO}_2](t) = [\text{ClNO}_2](t_0) + (\gamma \times f) \cdot \int_{t_0}^t \frac{C \cdot S_a}{4} [\text{N}_2\text{O}_5] dt \quad (\text{Eq. 3})$$

306 Here t_0 and t denote the start time and end time, respectively, the calculation time duration was
307 normally several hours. $[\text{ClNO}_2](t_0)$ is the observed concentration at t_0 and set as the fitting offset. Note
308 that the transportation leads to the bias of N₂O₅ uptake coefficient and ClNO₂ yield. But the small
309 variation of the mixing ratio of CO (< 5%) during each analysis time periods suggested the transport

310 process is not important to the increasing ClNO₂. The derived $\gamma \times f$ was found to be constant with small
311 uncertainties for optimization (see Table S3). The $\gamma \times f$ had moderate variability, ranged from 0.008 -
312 0.035 with an average of 0.019 ± 0.009 . Table 3 summarizes the $\gamma \times f$ values derived in the previous
313 field observations. The value in suburban Germany was between 0.001 and 0.09, with the average of
314 0.014 (Phillips et al., 2016), and the average value in Mt. Tai, China, was approximately 0.016 (Z.
315 Wang et al., 2017). The average $\gamma \times f$ in this study was comparable with that of the two suburban sites,
316 whereas in an urban site of Jinan, China (X. F. Wang et al., 2017), the value was lower than 0.008 and
317 comparable with that in the CalNex-LA campaign. The three sets of $\gamma \times f$ values from suburban regions
318 were about twice as large as those in urban regions, which implies that the ClNO₂ formation efficiency
319 in the aged air masses in suburban regions were more efficient than in the urban region. The difference
320 of the overall yield between the two regions may be caused by particle properties or other factors
321 (Riemer et al., 2009; Gaston et al., 2014; Grzanic et al., 2015; Bertram and Thornton, 2009).

322 According to reaction R4, soluble nitrate and ClNO₂ were formed by N₂O₅ heterogeneous uptake,
323 with yields of $2 - f$ and f , respectively. Following the recent work of Phillips et al., (2016), we used the
324 observed pNO₃⁻ and ClNO₂ formation rates to derive individual γ and f . The calculations assumed that
325 the relevant properties of the air mass are conserved and that the losses of produced species are
326 negligible; additionally, the N₂O₅ uptake coefficients and the ClNO₂ yield are independent of particle
327 size. The nights characterized by the following two features were chosen for further analysis: (1)
328 significant correlations between pNO₃⁻ and ClNO₂ were present ($R^2 > 0.5$), which suggested that, to a
329 good approximation, both ClNO₂ and pNO₃⁻ are produced only by N₂O₅ heterogeneous uptake. The
330 reason for excluding other nights with low correction ($R^2 < 0.2$) was ClNO₂ and pNO₃⁻ may be affected
331 by the effective transportation or other production pathways, and these contributions can't be well
332 quantified. Therefore the selection of high correction of ClNO₂ with pNO₃⁻ may be lead a bias as the
333 contribution from other formation pathways and the transportation were neglected. (2)
334 During an increasing period of pNO₃⁻, an equivalent or faster increase of ammonium molar ratio to
335 pNO₃⁻ was also observed, which means enough gas-phase ammonia was repartitioned
336 to form ammonium nitrate and suppress the release of HNO₃. The ammonia rich conditions (22 ± 9
337 ppbv on average) in Beijing demonstrated that the degassing of HNO₃ at night can be effectively
338 buffered by the high concentrations of ammonia presented in the NCP (Liu et al., 2017). Both the gas-
339 particle repartitioning of HNO₃ or nighttime produced HNO₃ will result in the overestimation of γ and
340 the underestimation of f . The daytime produced HNO₃ will be soon in a new equilibrium rapidly on
341 the time scale of total nitrate chemical production, and the nighttime formation of HNO₃ are normally
342 not important, so the nocturnal HNO₃ uptake impact is negligible. During this campaign, five nights
343 were eligible for the following analysis. Based on the observational data of N₂O₅, ClNO₂, pNO₃⁻ and
344 S_a in 5 minutes average. The formations of pNO₃⁻ and ClNO₂ were integrated to reproduce the
345 increasing pNO₃⁻ and ClNO₂ by input an initial γ and f . The offset of pNO₃⁻ and ClNO₂ is the measured
346 pNO₃⁻ and ClNO₂ concentration at the start time. The γ and f were optimized based on the Levenberg-
347 Marquardt algorithm until good agreement between the observed and predicted concentrations of
348 pNO₃⁻ and ClNO₂ was obtained (Phillips et al., 2016). Figure 5 depicts an example of the fitting results
349 on May 28. The predicted N₂O₅ uptake coefficient and ClNO₂ yield were 0.017 and 1.0, respectively.
350 The uncertainty on each individual fitting is varied from 55% - 100% due to the variability and
351 measurements uncertainties of pNO₃⁻ and ClNO₂. Five sets of values of γ and f obtained are listed in
352 Table 4. N₂O₅ uptake coefficients ranged from 0.012 - 0.055, with an average of 0.034 ± 0.018 , and

353 the ClNO₂ yield ranged from 0.50 to unity, with an average of 0.73 ± 0.25. The errors from each
354 derivation were 55% and came from the field measurements of S_a, N₂O₅, pNO₃⁻ and ClNO₂.

355 The average γ value was consistent with the results determined by the same method in a rural site in
356 Germany (Phillips et al., 2016), but was higher than those in the UK and North America where they
357 used other derivation methods, included the steady state lifetime method (Morgan et al., 2015; Brown
358 et al., 2006, 2009), the iterated box model (Wagner et al., 2013) and direct measurement based on an
359 aerosol flow reactor (Bertram et al., 2009; Riedel et al., 2012). The steady state lifetime method is very
360 sensitive to NO₂ concentration, and since the NO₂ measurement suffered with ambient NO_y
361 interference, we did not apply the steady state lifetime method in this study (Brown et al., 2003).
362 Nonetheless, the derived γ in Beijing showed good agreement with the recent results derived by the
363 steady state method in Jinan and Mt. Tai (X. F. Wang et al., 2017; Z. Wang et al., 2017). The
364 consistency eliminates the discrepancy possibly brought by the differences of analysis methods.
365 Therefore, we suggest that fast N₂O₅ uptake was a ubiquitous feature that existed in the NCP. In this
366 study, sulfate is the dominant component of PM_{1.0}, accounting for more than 30% of its mass
367 concentration, which may be the reason of elevated N₂O₅ uptake coefficient presented in Beijing, like
368 the result in high sulfate air mass over Ohio and western Pennsylvania (Brown et al., 2006). Previous
369 studies have shown that the N₂O₅ uptake coefficient strongly depends on the liquid water content, the
370 pNO₃⁻ and organic mass. Liquid water content promotes N₂O₅ uptake, whereas pNO₃⁻ and organic
371 mass inhibit N₂O₅ uptake (e.g., Thornton et al., 2003, Wahner et al., 1998; Bertram and Thornton,
372 2009). Because of the limited data set of N₂O₅ uptake coefficients in this work, the function
373 dependence studies about the determined N₂O₅ uptake coefficients with the parameters mentioned
374 above were not convincing. More valid data are needed in the further studies of the N₂O₅ uptake
375 mechanism. With respect to f , the values are comparable with that observed in Germany (Phillips et
376 al., 2016) and are similar to that estimated in the power plant plume in Mt. Tai with high chloride
377 content (Z. Wang et al., 2017).

378 4.2 N₂O₅ lifetime and reactivity

379 The lifetime of N₂O₅ was estimated by the steady state method, assuming that the production and loss
380 of N₂O₅ was in balance after a period following sunset. Eq. 4 for the steady state approximation has
381 been frequently applied in analyzing the fate of N₂O₅ (Platt et al., 1980; Allan et al., 1999; Brown et
382 al., 2003).

$$383 \quad \tau_{ss}(\text{N}_2\text{O}_5) = \frac{1}{L_{ss}(\text{N}_2\text{O}_5)} = \frac{[\text{N}_2\text{O}_5]}{k_{\text{NO}_2+\text{O}_3}[\text{NO}_2][\text{O}_3]} \quad (\text{Eq. 4})$$

384 Here $\tau_{ss}(\text{N}_2\text{O}_5)$ denotes the steady state lifetime of N₂O₅ and $L_{ss}(\text{N}_2\text{O}_5)$ denotes the loss term of N₂O₅
385 corresponding to the steady state lifetime. A numerical model was used to check the validity of the
386 steady state approximation (Brown et al., 2003); details are given in Figure S3. The results show that
387 the steady state can generally be achieved within 30 minutes. In this study, the steady state lifetime
388 was only calculated from 20:00 to the next day 04:00. The time periods with NO concentration larger
389 than 0.06 ppbv (instrument LOD) were excluded as the steady state is easily disturbed. The overall
390 N₂O₅ loss rate ($k(\text{N}_2\text{O}_5)$) can be calculated by accumulating each individual loss term in Eq. 5,
391 including the N₂O₅ heterogeneous hydrolysis and the reaction of NO₃ with VOCs.

$$k(\text{N}_2\text{O}_5) = \frac{\sum k_{\text{NO}_3+\text{VOC}_i} \cdot [\text{VOC}_i]}{k_{\text{eq}} \cdot [\text{NO}_2]} + \frac{C \cdot S_a \cdot \gamma}{4} \quad (\text{Eq. 5})$$

393 The NO_3 heterogeneous uptake and the loss of N_2O_5 via gas-phase reactions were assumed to be
 394 negligible (Brown and Stutz, 2012). $k_{\text{NO}_3+\text{VOC}_i}$ denotes the reaction rate constants of the reaction of
 395 NO_3+VOC_i . Isoprene and monoterpene were used in this calculation.

396 The N_2O_5 loss rate coefficient by heterogeneous hydrolysis was calculated by using an average γ of
 397 0.034. The time series of the steady state lifetime of N_2O_5 is shown in Figure S4. The N_2O_5 steady state
 398 lifetime ranged from <5 s to 1260 s, with an average of 270 ± 240 s, and large variability was shown
 399 during the campaign. The N_2O_5 lifetimes during the BAM period were higher than those during the
 400 UAM period, which is predictable since the clean air mass has lower N_2O_5 reactivity because of much
 401 lower aerosol loading. Two extremely short N_2O_5 lifetime cases were captured on the nights of May
 402 30 and June 3, with peak values below 200 s throughout those nights. Figure 6 shows that the N_2O_5
 403 lifetime had a very clear negative dependence on the ambient S_a when larger than $300 \mu\text{m}^2 \text{cm}^{-3}$, which
 404 indicates that the N_2O_5 heterogeneous uptake plays an important role in the regulation of N_2O_5 lifetime.
 405 The study conducted in the residual layer of Hong Kong showed a similar tendency despite the overall
 406 N_2O_5 lifetime being shorter at this site (Brown et al., 2016). Additionally, a negative dependence of
 407 N_2O_5 lifetime on RH was reported in Hong Kong but was not observed in this study (Figure S5).

408 Figure 7 shows the time series of the overall N_2O_5 loss rate constant as well as the N_2O_5 steady state
 409 loss rate constant. The overall N_2O_5 loss rate constant was calculated from the individual terms (Eq.3).
 410 The uncertainties of the N_2O_5 steady state loss rate constant and the overall $k(\text{N}_2\text{O}_5)$ are estimated to
 411 be 67% and 95%, respectively (Eq. 6 and Eq. 7). The largest error sources were from the corrected
 412 NO_2 measurements.

$$413 \frac{\Delta L_{SS}(\text{N}_2\text{O}_5)}{L_{SS}(\text{N}_2\text{O}_5)} = \sqrt{\left(\frac{\Delta[\text{N}_2\text{O}_5]}{[\text{N}_2\text{O}_5]}\right)^2 + \left(\frac{\Delta[\text{NO}_2]}{[\text{NO}_2]}\right)^2 + \left(\frac{\Delta[\text{O}_3]}{[\text{O}_3]}\right)^2 + \left(\frac{\Delta K_{\text{eq}}}{K_{\text{eq}}}\right)^2} \quad (\text{Eq. 6})$$

$$414 \frac{\Delta k(\text{N}_2\text{O}_5)}{k(\text{N}_2\text{O}_5)} = \sqrt{\left(\frac{\Delta[\text{N}_2\text{O}_5]}{[\text{N}_2\text{O}_5]}\right)^2 + \left(\frac{\Delta[S_a]}{[S_a]}\right)^2 + \left(\frac{\Delta[\gamma]}{[\gamma]}\right)^2 + \left(\frac{\Delta[\text{NO}_2]}{[\text{NO}_2]}\right)^2 + \left(\frac{\Delta[\text{O}_3]}{[\text{O}_3]}\right)^2 + \left(\frac{\Delta[\text{VOC}_i]}{[\text{VOC}_i]}\right)^2 + \left(\frac{\Delta K_{\text{eq}}}{K_{\text{eq}}}\right)^2} \quad (\text{Eq. 7})$$

415 On the night of 29 May, the steady state loss rate constant was much lower than the overall $k(\text{N}_2\text{O}_5)$;
 416 on the nights of 28, May and 3 June, the $L_{SS}(\text{N}_2\text{O}_5)$ calculated by the steady state method were much
 417 higher than the overall $k(\text{N}_2\text{O}_5)$, but these discrepancies were in the range of the uncertainties. The
 418 steady state loss rate constant in the case of May 30 was approximately ten times larger than the overall
 419 loss rate constant, and this difference was outside of the range of uncertainty. The reason for the larger
 420 difference on this night is not understood from the available measurements. In general, the overall
 421 N_2O_5 loss rate constant and the steady state N_2O_5 loss rate constant were comparable taking into
 422 considerations of the uncertainties. The average N_2O_5 loss rate constant contributed by the N_2O_5
 423 heterogeneous hydrolysis was $8.1 \times 10^{-4} \text{ s}^{-1}$. The average NO_3 loss rate constant by the reaction of NO_3
 424 with VOCs was $0.015 \pm 0.007 \text{ s}^{-1}$, which is comparable with the previous results in suburban Beijing
 425 in 2006 (H. C. Wang et al., 2017c), in which the contribution to the N_2O_5 reactivity was $1.63 \times 10^{-3} \pm$
 426 $0.65 \times 10^{-3} \text{ s}^{-1}$ on average. Compared with N_2O_5 loss via direct heterogeneous hydrolysis, the indirect
 427 loss via NO_3+VOC_i was dominant, accounting for approximately 67%. Because only a subset of the

428 suite of organic species at the site was measured, the calculated loss rate constant via NO_3+VOCs
429 represents a lower limit. Therefore, the N_2O_5 loss via NO_3+VOCs may occupy a larger proportion. The
430 overall loss rate constant from NO_3+VOCs and N_2O_5 uptake was $2.44\times 10^{-3} \pm 1.5\times 10^{-3} \text{ s}^{-1}$ on average,
431 which was reasonably lower than the steady state N_2O_5 loss rate constant of $3.61\times 10^{-3} \pm 2.80\times 10^{-3} \text{ s}^{-1}$
432 on average. The gap may be explained by the unmeasured reactive VOCs or the unaccounted NO that
433 was near the instrumental limit of detection.

434 4.3 NO_3 -induced nocturnal oxidation of VOCs

435 Recent studies have suggested that the fate of BVOCs after sunset is dominated by NO_x or O_3 , with
436 variation of the ratio of NO_x to BVOCs and that the nighttime oxidation is located in the transition
437 region between NO_x -domination and O_3 -domination in the United States (Edwards et al., 2017).
438 During this campaign, the nocturnal average concentrations of isoprene and monoterpene were $156 \pm$
439 88 pptv and 86 ± 42 pptv, respectively. We used isoprene and monoterpene to represent a lower limit
440 mixing ratio of total BVOCs; the average ratio of NO_x/BVOCs was larger than 10 and exhibited small
441 variation during the BAM and UAM periods. The value was much higher than the critical value (NO_x
442 $/\text{BVOC} = 0.5$) of the transition regime proposed by Edwards et al. (2017), which suggests that the
443 oxidation of BVOCs in Beijing was NO_x -dominated and the nighttime fate of BVOCs was controlled
444 by NO_3 . Since the reaction of NO_3 with BVOCs has a high mass yield, the nocturnal ON production
445 may be important in the high NO_x/BVOCs region.

446 The first order loss rate of VOCs ~~initialized~~ by oxidants, $k(\text{VOCs}_i)$, is defined as VOCs
447 reactivity and expressed as Eq. 8. Here, we only consider the reaction of VOCs with O_3 and NO_3 .
448 $k_{\text{O}_3+\text{VOCs}_i}$ denotes the reaction rate constants of VOCs_i with O_3 .

$$449 \quad k(\text{VOCs}_i) = k_{\text{NO}_3+\text{VOCs}_i} \cdot [\text{NO}_3] + k_{\text{O}_3+\text{VOCs}_i} \cdot [\text{O}_3] \quad (\text{Eq. 8})$$

450 During this campaign, VOCs reactivity could be determined with the measured O_3 and calculated NO_3 .
451 Figure 8 depicts four kinds of VOCs reactivity distribution during nighttime, including the isoprene
452 (ISO), monoterpene (MNT), the double bond at the end or terminal position of the molecule (OLT)
453 and alkenes with the double bond elsewhere in the molecule (OLI). The reaction rates were cited from
454 the regional atmospheric chemistry mechanism version 2 (RACM2, Goliff et al., (2013)). Previous
455 measurement indicated the main detectable monoterpenes were α -pinene and β -pinene in summer
456 Beijing (personal communication with Ying Liu). Here we assumed α -pinene and β -pinene occupies
457 half and half in the monoterpene with ~~an uncertainty the amount quantification uncertainty~~ of 50%.
458 The rate coefficients of α -pinene and β -pinene with NO_3 were referred to Atkinson and Arey, (2003).
459 The uncertainty of calculated mixing ratio of NO_3 is 67%, and the overall uncertainty of monoterpene
460 reactivity was calculated to be 85% by Gaussian propagation. The uncertainties of other kinds of VOCs
461 was calculated to be 75% by assuming the uncertainty of rate coefficient was 30%. The VOCs
462 reactivity were dominated by NO_3 oxidation and contributed up to 90% in total; less than 10% VOCs
463 were oxidized by O_3 during the nighttime. Even the NO_3 concentration in the lower range, NO_3 still
464 responsible for more than 70% nocturnal BVOCs oxidation, the results further confirmed that the
465 oxidation of BVOCs is controlled by NO_3 rather than O_3 in summer Beijing.

466 For calculating nocturnal ON production from NO_3 oxidation of isoprene and monoterpene, as well
467 as inorganic nitrate production via N_2O_5 heterogeneous uptake over the same period, the ClNO_2 yield
468 was set to the determined average value of 0.55. The organic nitrate yield of the reaction of NO_3 with
469 isoprene was set to 0.7, from Rollins et al. (2009). The yield from the reaction of NO_3 with
470 monoterpene was represented by $\text{NO}_3 + \alpha$ -pinene and was set to 0.16, following Spittler et al. (2006).
471 As the α -pinene and β -pinene have very different ON yields, the yield set in the study was an upper
472 limit for α -pinene initiated ON, but is relative low yield for the β -pinene ~~initialized~~ ON (e.g.,
473 Hallquist et al., 1999). Although the yield from the NO_3 oxidation of isoprene is much higher than that
474 of monoterpene, the total ON production was dominated by the oxidation of NO_3 with monoterpene
475 because the reaction of NO_3 with monoterpene is much faster than that with isoprene. Because of the
476 lack of measurement of alkenes and other VOCs that can react with NO_3 and form ON, the calculated
477 nighttime ON production rate analyzed here served as a lower estimations.

478 Figure 9 depicts the mean diurnal profiles of the nocturnal formation rates of inorganic nitrates and
479 ON. The average production rate of ON was up to 0.10 ± 0.07 ppbv h^{-1} , which was higher than that
480 predicted in a suburban site in Beijing in 2006, with an average value of 0.06 ppbv h^{-1} (H.C. Wang et
481 al., 2017b). In the high NO_x/BVOCs air masses, the inorganic nitrate formation was proposed to
482 increase with the increase of sunset NO_x/BVOCs (Edwards et al., 2017). The formation rate of
483 inorganic nitrate via N_2O_5 uptake was significant, with an average of 0.43 ± 0.12 ppbv h^{-1} , and was
484 much larger than the ON formation. NO_x was mainly removed as the inorganic nitrate format by
485 nocturnal NO_3 - N_2O_5 chemistry in Beijing. Overall, the NO_3 - N_2O_5 chemistry led to significant NO_x
486 removal, with 0.54 ppbv h^{-1} accounted for by the organic and inorganic nitrates, and the integral NO_x
487 removal was approximately 5 ppbv per night. Since ON are important precursors of the secondary
488 organic aerosols (SOA), the NO_3 oxidation was very important from the perspective of organic aerosol
489 formation and regional particulate matter (e.g., Ng et al., 2008).

490 5. Conclusion

491 We reported an intensive field study of NO_3 - N_2O_5 chemistry at a downwind suburban site in Beijing
492 during the summer of 2016. High levels of ClNO_2 and N_2O_5 were observed, with maxima of 2.9 ppbv
493 and 937 pptv (1-min), respectively. The N_2O_5 uptake coefficient was estimated to be in the range of
494 0.010-0.055, with an average value of 0.034 ± 0.018 , and the corresponding ClNO_2 yield was derived
495 to be in the range of 0.5-1.0, with an average value of 0.73 ± 0.25 . The elevated ClNO_2 levels and
496 $\text{ClNO}_2/\text{N}_2\text{O}_5$ ratios are comparable with those in chloride-rich regions in the NCP. The results highlight
497 fast N_2O_5 heterogeneous hydrolysis and efficient ClNO_2 formation in the outflow of urban Beijing.

498 Since the NO_3 - N_2O_5 chemical equilibrium favors NO_3 in summer with high temperature, the
499 elevated NO_3 dominated the nocturnal degradation of BVOCs and could lead to efficient ON formation.
500 Because the air masses in Beijing featured high NO_x/BVOCs ratios (>10), our results suggest that the
501 nocturnal NO_3 oxidation of BVOCs was NO_x -dominated. Because of the extremely high NO_x
502 emissions, the formation of ON may not be sensitive to the reduction of NO_x but rather to the change
503 of unsaturated VOCs (e.g., BVOCs), which is similar to the daytime photochemical O_3 pollution (e.g.,
504 Lu et al., 2010) diagnosed for this area. This suggests that the control of the unsaturated VOCs would
505 moderate the O_3 pollution and ON particulate matter in parallel. Moreover, the reduction of NO_x would

506 also be helpful to reduce the pNO_3^- formation via N_2O_5 heterogeneous hydrolysis under such high
507 NO_x/BVOCs ratios (Edwards et al., 2017).

508

509 **Acknowledgements.** This work was supported by the National Natural Science Foundation of China
510 (Grants No. 91544225, 41375124, 21522701, 41421064, 91744204), the National Science and
511 Technology Support Program of China (No. 2014BAC21B01), the Strategic Priority Research
512 Program of the Chinese Academy of Sciences (Grants No. XDB05010500), and the program on
513 “Photochemical smog in China” financed by the Swedish Research Council (639-2013-6917). The
514 authors gratefully acknowledge the Peking University and Gethenburg University science team for
515 their technical support and discussions during the Changping campaign.

516

517 **Reference**

518

519 Allan, B. J., Carslaw, N., Coe, H., Burgess, R. A., and Plane, J. M. C.: Observations of the nitrate radical in the marine
520 boundary layer, *J Atmos Chem*, 33, 129-154, Doi10.1023/A:1005917203307, 1999.

521 Bannan, T. J., Booth, A. M., Bacak, A., Muller, J. B. A., Leather, K. E., Le Breton, M., Jones, B., Young, D., Coe, H.,
522 Allan, J., Visser, S., Slowik, J. G., Furger, M., Prevot, A. S. H., Lee, J., Dunmore, R. E., Hopkins, J. R., Hamilton,
523 J. F., Lewis, A. C., Whalley, L. K., Sharp, T., Stone, D., Heard, D. E., Fleming, Z. L., Leigh, R., Shallcross, D.
524 E., and Percival, C. J.: The first UK measurements of nitryl chloride using a chemical ionization mass
525 spectrometer in central London in the summer of 2012, and an investigation of the role of Cl atom oxidation, *J*
526 *Geophys Res-Atmos*, 120, 5638-5657, 10.1002/2014jd022629, 2015.

527 Benton, A. K., Langridge, J. M., Ball, S. M., Bloss, W. J., Dall'Osto, M., Nemitz, E., Harrison, R. M., and Jones, R.
528 L.: Night-time chemistry above London: measurements of NO_3 and N_2O_5 from the BT Tower, *Atmos Chem*
529 *Phys*, 10, 9781-9795, 10.5194/acp-10-9781-2010, 2010.

530 Bertram, T. H., and Thornton, J. A.: Toward a general parameterization of N_2O_5 reactivity on aqueous particles: the
531 competing effects of particle liquid water, nitrate and chloride, *Atmos Chem Phys*, 9, 8351-8363, 2009.

532 Bertram, T. H., Thornton, J. A., Riedel, T. P., Middlebrook, A. M., Bahreini, R., Bates, T. S., Quinn, P. K., and
533 Coffman, D. J.: Direct observations of N_2O_5 reactivity on ambient aerosol particles, *Geophys Res Lett*, 36, Art
534 L19803.10.1029/2009gl040248, 2009.

535 Bohn, B., Corlett, G. K., Gillmann, M., Sanghavi, S., Stange, G., Tensing, E., Vrekoussis, M., Bloss, W. J., Clapp, L.
536 J., Kortner, M., Dorn, H.-P., Monks, P. S., Platt, U., Plass-Dülmer, C., Mihalopoulos, N., Heard, D. E.,
537 Clemmitshaw, K. C., Meixner, F. X., Prevot, A. S. H., and Schmitt, R.: Photolysis frequency measurement
538 techniques: results of a comparison within the ACCENT project, *Atmos. Chem. Phys.*, 8, 5373–5391,
539 doi:10.5194/acp-8-5373-2008, 2008.

540 Behnke, W., George, C., Scheer, V., and Zetzsch, C.: Production and decay of ClNO_2 , from the reaction of gaseous
541 N_2O_5 with NaCl solution: Bulk and aerosol experiments, *J Geophys Res-Atmos*, 102, 3795-3804, Doi
542 10.1029/96jd03057, 1997.

543 Boyd, C. M., Nah, T., Xu, L., Berkemeier, T., and Ng, N. L.: Secondary Organic Aerosol (SOA) from Nitrate Radical
544 Oxidation of Monoterpenes: Effects of Temperature, Dilution, and Humidity on Aerosol Formation, Mixing,
545 and Evaporation, *Environ Sci Technol*, 51, 7831-7841, 2017.

546 Brown, S. S., Stark, H., and Ravishankara, A. R.: Applicability of the steady state approximation to the interpretation
547 of atmospheric observations of NO₃ and N₂O₅, *J Geophys Res-Atmos*, 108, Artn 4539. Doi
548 10.1029/2003jd003407, 2003.

549 Brown, S. S., Ryerson, T. B., Wollny, A. G., Brock, C. A., Peltier, R., Sullivan, A. P., Weber, R. J., Dube, W. P.,
550 Trainer, M., Meagher, J. F., Fehsenfeld, F. C., and Ravishankara, A. R.: Variability in nocturnal nitrogen oxide
551 processing and its role in regional air quality, *Science*, 311, 67-70, DOI 10.1126/science.1120120, 2006.

552 Brown, S. S., Dube, W. P., Fuchs, H., Ryerson, T. B., Wollny, A. G., Brock, C. A., Bahreini, R., Middlebrook, A. M.,
553 Neuman, J. A., Atlas, E., Roberts, J. M., Osthoff, H. D., Trainer, M., Fehsenfeld, F. C., and Ravishankara, A. R.:
554 Reactive uptake coefficients for N₂O₅ determined from aircraft measurements during the Second Texas Air
555 Quality Study: Comparison to current model parameterizations, *J Geophys Res-Atmos*, 114, Artn D00f10. Doi
556 10.1029/2008jd011679, 2009.

557 Brown, S. S., and Stutz, J.: Nighttime radical observations and chemistry, *Chem Soc Rev*, 41, 6405-6447, Doi
558 10.1039/C2cs35181a, 2012.

559 Brown, S. S., Dube, W. P., Tham, Y. J., Zha, Q. Z., Xue, L. K., Poon, S., Wang, Z., Blake, D. R., Tsui, W., Parrish, D.
560 D., and Wang, T.: Nighttime chemistry at a high altitude site above Hong Kong, *J Geophys Res-Atmos*, 121,
561 2457-2475, 10.1002/2015jd024566, 2016.

562 Chang, W. L., Bhave, P. V., Brown, S. S., Riemer, N., Stutz, J., and Dabdub, D.: Heterogeneous Atmospheric
563 Chemistry, Ambient Measurements, and Model Calculations of N₂O₅: A Review, *Aerosol Sci Tech*, 45, 665-695,
564 2011.

565 DeCarlo, P. F., Kimmel, J., Trimborn, A., Northway, M., Jayne, J. T., Aiken, A., Gonin, M., Fuhrer, K., Horvath, T.,
566 Docherty, K., Worsnop, D. R., and Jimenez, J. L.: Field-deployable, high-resolution, time-of-flight Aerosol Mass
567 Spectrometer, *Anal. Chem.*, 78, 8281-8289, 2006.

568 de Gouw, J. and Warneke, C.: Measurements of volatile organic compounds in the earth's atmosphere using proton-
569 transferreaction mass spectrometry, *Mass Spectrom. Rev.*, 26, 223-257, 2007.

570 Draxler, R. R., and G. D. Rolph: HYSPLIT (HYbrid Single-Particle Lagrangian Integrated Tracker) Model access
571 via NOAA ARL Ready Website [Available at <http://www.arl.noaa.gov/ready/hysplit4.html>, NOAA Air
572 Resources Laboratory, Silver Spring, MD]. 2003.

573 Edwards, P. M., Aikin, K. C., Dube, W. P., Fry, J. L., Gilman, J. B., de Gouw, J. A., Graus, M. G., Hanisco, T. F.,
574 Holloway, J., Huber, G., Kaiser, J., Keutsch, F. N., Lerner, B. M., Neuman, J. A., Parrish, D. D., Peischl, J.,
575 Pollack, I. B., Ravishankara, A. R., Roberts, J. M., Ryerson, T. B., Trainer, M., Veres, P. R., Wolfe, G. M.,
576 Warneke, C., and Brown, S. S.: Transition from high- to low-NO_x control of night-time oxidation in the
577 southeastern US, *Nat Geosci*, 10, 490+, 10.1038/Ngeo2976, 2017.

578 Faxon, C. B., Bean, J. K., and Ruiz, L. H.: Inland Concentrations of Cl₂ and ClNO₂ in Southeast Texas suggest
579 chlorine chemistry significantly contributes to atmospheric reactivity, *Atmosphere*, 6, 1487-1506, 2015.

580 Finlayson-Pitts, B. J., Ezell, M. J., and Pitts, J. N.: Formation of Chemically Active Chlorine Compounds by
581 Reactions of Atmospheric NaCl Particles with Gaseous N_2O_5 and ClONO_2 , *Nature*, 337, 241-244, DOI
582 10.1038/337241a0, 1989.

583 Fry, J. L., Kiendler-Scharr, A., Rollins, A. W., Wooldridge, P. J., Brown, S. S., Fuchs, H., Dube, W., Mensah, A., dal
584 Maso, M., Tillmann, R., Dorn, H. P., Brauers, T., and Cohen, R. C.: Organic nitrate and secondary organic
585 aerosol yield from NO_3 oxidation of beta-pinene evaluated using a gas-phase kinetics/aerosol partitioning model,
586 *Atmos Chem Phys*, 9, 1431-1449, 2009.

587 Gaston, C. J., Thornton, J. A., and Ng, N. L.: Reactive uptake of N_2O_5 to internally mixed inorganic and organic
588 particles: the role of organic carbon oxidation state and inferred organic phase separations, *Atmos Chem Phys*,
589 14, 5693-5707, 10.5194/acp-14-5693-2014, 2014.

590 Geyer, A., Aliche, B., Konrad, S., Schmitz, T., Stutz, J., and Platt, U.: Chemistry and oxidation capacity of the nitrate
591 radical in the continental boundary layer near Berlin, *J Geophys Res-Atmos*, 106, 8013-8025, Doi
592 10.1029/2000jd900681, 2001.

593 Goliff, W. S., Stockwell, W. R., and Lawson, C. V.: The regional atmospheric chemistry mechanism, version 2, *Atmos*
594 *Environ*, 68, 174-185, 2013.

595 Grzinic, G., Bartels-Rausch, T., Berkemeier, T., Turler, A., and Ammann, M.: Viscosity controls humidity dependence
596 of N_2O_5 uptake to citric acid aerosol, *Atmos Chem Phys*, 15, 13615-13625, 2015.

597 Hallquist, M., Stewart, D. J., Stephenson, S. K., and Cox, R. A.: Hydrolysis of N_2O_5 on sub-micron sulfate aerosols,
598 *Phys Chem Chem Phys*, 5, 3453-3463, Doi 10.1039/B301827j, 2003.

599 Hallquist, M., Munthe, J., Hu, M., Wang, T., Chan, C. K., Gao, J., Boman, J., Guo, S., Hallquist, A. M., Mellqvist, J.,
600 Moldanova, J., Pathak, R. K., Pettersson, J. B. C., Pleijel, H., Simpson, D., and Thynell, M.: Photochemical
601 smog in China: scientific challenges and implications for air-quality policies, *Natl Sci Rev*, 3, 401-403,
602 10.1093/nsr/nww080, 2016.

603 Kiendler-Scharr, A., Mensah, A. A., Friese, E., Topping, D., Nemitz, E., Prevot, A. S. H., Aijala, M., Allan, J.,
604 Canonaco, F., Canagaratna, M., Carbone, S., Crippa, M., Dall'Osto, M., Day, D. A., De Carlo, P., Di Marco, C.
605 F., Elbern, H., Eriksson, A., Freney, E., Hao, L., Herrmann, H., Hildebrandt, L., Hillamo, R., Jimenez, J. L.,
606 Laaksonen, A., McFiggans, G., Mohr, C., O'Dowd, C., Otjes, R., Ovadnevaite, J., Pandis, S. N., Poulain, L.,
607 Schlag, P., Sellegri, K., Swietlicki, E., Tiitta, P., Vermeulen, A., Wahner, A., Worsnop, D., and Wu, H. C.:
608 Ubiquity of organic nitrates from nighttime chemistry in the European submicron aerosol, *Geophys Res Lett*,
609 43, 7735-7744, 2016.

610 Le Breton, M., Bacak, A., Muller, J. B. A., Bannan, T. J., Kennedy, O., Ouyang, B., Xiao, P., Bauguitte, S. J. B.,
611 Shallcross, D. E., Jones, R. L., Daniels, M. J. S., Ball, S. M., and Percival, C. J.: The first airborne comparison
612 of N_2O_5 measurements over the UK using a CIMS and BBCEAS during the RONOCO campaign, *Anal*
613 *Methods-Uk*, 6, 9731-9743, 10.1039/c4ay02273d, 2014.

614 Le Breton, M., Hallquist, Å. M., Pathak, R. K., Simpson, D., Wang, Y., Johansson, J., Zheng, J., Yang, Y., Shang, D.,
615 Wang, H., Liu, Q., Chan, C., Wang, T., Bannan, T. J., Priestley, M., Percival, C. J., Shallcross, D. E., Lu, K.,
616 Guo, S., Hu, M., and Hallquist, M.: Chlorine oxidation of VOCs at a semi-rural site in Beijing: Significant

617 chlorine liberation from ClNO₂ and subsequent gas and particle phase Cl-VOC production, *Atmos. Chem. Phys.*
618 *Discuss.*, 2018, 1-25, 2018.

619 Li, S. W., Liu, W. Q., Xie, P. H., Qin, M., and Yang, Y. J.: Observation of Nitrate Radical in the Nocturnal Boundary
620 Layer During a Summer Field Campaign in Pearl River Delta, China, *Terr Atmos Ocean Sci*, 23, 39-48, Doi
621 10.3319/Tao.2011.07.26.01(a), 2012.

622 Li, Q. Y., Zhang, L., Wang, T., Tham, Y. J., Ahmadov, R., Xue, L. K., Zhang, Q., and Zheng, J. Y.: Impacts of
623 heterogeneous uptake of dinitrogen pentoxide and chlorine activation on ozone and reactive nitrogen
624 partitioning: improvement and application of the WRF-Chem model in southern China, *Atmos Chem Phys*, 16,
625 14875-14890, 10.5194/acp-16-14875-2016, 2016.

626 Liu, X. G., Gu, J. W., Li, Y. P., Cheng, Y. F., Qu, Y., Han, T. T., Wang, J. L., Tian, H. Z., Chen, J., and Zhang, Y. H.:
627 Increase of aerosol scattering by hygroscopic growth: Observation, modeling, and implications on visibility,
628 *Atmos Res*, 132, 91-101, 10.1016/j.atmosres.2013.04.007, 2013.

629 Liu, M. X., Song, Y., Zhou, T., Xu, Z. Y., Yan, C. Q., Zheng, M., Wu, Z. J., Hu, M., Wu, Y. S., and Zhu, T.: Fine
630 particle pH during severe haze episodes in northern China, *Geophys Res Lett*, 44, 5213-5221,
631 10.1002/2017gl073210, 2017.

632 Lopez-Hilfiker, F. D., Mohr, C., Ehn, M., Rubach, F., Kleist, E., Wildt, J., Mentel, T. F., Lutz, A., Hallquist, M.,
633 Worsnop, D., and Thornton, J. A.: A novel method for online analysis of gas and particle composition:
634 description and evaluation of a Filter Inlet for Gases and AEROSols (FIGAERO), *Atmos Meas Tech*, 7, 983-
635 1001, 10.5194/amt-7-983-2014, 2014.

636 Lu, K. D., Zhang, Y. H., Su, H., Brauers, T., Chou, C. C., Hofzumahaus, A., Liu, S. C., Kita, K., Kondo, Y., Shao,
637 M., Wahner, A., Wang, J. L., Wang, X. S., and Zhu, T.: Oxidant (O₃ + NO₂) production processes and formation
638 regimes in Beijing, *J Geophys Res-Atmos*, 115, 2010.

639 McLaren, R., Wojtal, P., Majonis, D., McCourt, J., Halla, J. D., and Brook, J.: NO₃ radical measurements in a polluted
640 marine environment: links to ozone formation, *Atmos Chem Phys*, 10, 4187-4206, 10.5194/acp-10-4187-2010,
641 2010.

642 Mentel, T. F., Sohn, M., and Wahner, A.: Nitrate effect in the heterogeneous hydrolysis of dinitrogen pentoxide on
643 aqueous aerosols, *Phys Chem Chem Phys*, 1, 5451-5457, Doi 10.1039/A905338g, 1999.

644 Mielke, L. H., Furgeson, A., and Osthoff, H. D.: Observation of ClNO₂ in a Mid-Continental Urban Environment,
645 *Environ Sci Technol*, 45, 8889-8896, 10.1021/es201955u, 2011.

646 Mielke, L. H., Stutz, J., Tsai, C., Hurlock, S. C., Roberts, J. M., Veres, P. R., Froyd, K. D., Hayes, P. L., Cubison, M.
647 J., Jimenez, J. L., Washenfelder, R. A., Young, C. J., Gilman, J. B., de Gouw, J. A., Flynn, J. H., Grossberg, N.,
648 Lefer, B. L., Liu, J., Weber, R. J., and Osthoff, H. D.: Heterogeneous formation of nitryl chloride and its role as
649 a nocturnal NO_x reservoir species during CalNex-LA 2010, *J Geophys Res-Atmos*, 118, 10638-10652, Doi
650 10.1002/Jgrd.50783, 2013.

651 Morgan, W. T., Ouyang, B., Allan, J. D., Aruffo, E., Di Carlo, P., Kennedy, O. J., Lowe, D., Flynn, M. J., Rosenberg,
652 P. D., Williams, P. I., Jones, R., McFiggans, G. B., and Coe, H.: Influence of aerosol chemical composition on

653 N₂O₅ uptake: airborne regional measurements in northwestern Europe, *Atmos Chem Phys*, 15, 973-990, DOI
654 10.5194/acp-15-973-2015, 2015.

655 Ng, N. L., Kwan, A. J., Surratt, J. D., Chan, A. W. H., Chhabra, P. S., Sorooshian, A., Pye, H. O. T., Crouse, J. D.,
656 Wennberg, P. O., Flagan, R. C., and Seinfeld, J. H.: Secondary organic aerosol (SOA) formation from reaction
657 of isoprene with nitrate radicals (NO₃), *Atmos Chem Phys*, 8, 4117-4140, 2008.

658 Ng, N. L., Brown, S. S., Archibald, A. T., Atlas, E., Cohen, R. C., Crowley, J. N., Day, D. A., Donahue, N. M., Fry,
659 J. L., Fuchs, H., Griffin, R. J., Guzman, M. I., Herrmann, H., Hodzic, A., Iinuma, Y., Jimenez, J. L., Kiendler-
660 Scharr, A., Lee, B. H., Luecken, D. J., Mao, J. Q., McLaren, R., Mutzel, A., Osthoff, H. D., Ouyang, B., Picquet-
661 Varrault, B., Platt, U., Pye, H. O. T., Rudich, Y., Schwantes, R. H., Shiraiwa, M., Stutz, J., Thornton, J. A.,
662 Tilgner, A., Williams, B. J., and Zaveri, R. A.: Nitrate radicals and biogenic volatile organic compounds:
663 oxidation, mechanisms, and organic aerosol, *Atmos Chem Phys*, 17, 2103-2162, 10.5194/acp-17-2103-2017,
664 2017.

665 Osthoff, H. D., Roberts, J. M., Ravishankara, A. R., Williams, E. J., Lerner, B. M., Sommariva, R., Bates, T. S.,
666 Coffman, D., Quinn, P. K., Dibb, J. E., Stark, H., Burkholder, J. B., Talukdar, R. K., Meagher, J., Fehsenfeld, F.
667 C., and Brown, S. S.: High levels of nitryl chloride in the polluted subtropical marine boundary layer, *Nat Geosci*,
668 1, 324-328, Doi 10.1038/Ngeo177, 2008.

669 Phillips, G. J., Thieser, J., Tang, M. J., Sobanski, N., Schuster, G., Fachinger, J., Drewnick, F., Borrmann, S.,
670 Bingemer, H., Lelieveld, J., and Crowley, J. N.: Estimating N₂O₅ uptake coefficients using ambient
671 measurements of NO₃, N₂O₅, ClNO₂ and particle-phase nitrate, *Atmos Chem Phys*, 16, 13231-13249,
672 10.5194/acp-16-13231-2016, 2016.

673 Platt, U., Perner, D., Winer, A. M., Harris, G. W., and Pitts, J. N.: Detection of NO₃ in the Polluted Troposphere by
674 Differential Optical-Absorption, *Geophys Res Lett*, 7, 89-92, Doi 10.1029/G1007i001p00089, 1980.

675 Pye, H. O. T., Chan, A. W. H., Barkley, M. P., and Seinfeld, J. H.: Global modeling of organic aerosol: the importance
676 of reactive nitrogen (NO_x and NO₃), *Atmos Chem Phys*, 10, 11261-11276, 2010.

677 Riedel, T. P., Bertram, T. H., Ryder, O. S., Liu, S., Day, D. A., Russell, L. M., Gaston, C. J., Prather, K. A., and
678 Thornton, J. A.: Direct N₂O₅ reactivity measurements at a polluted coastal site, *Atmos Chem Phys*, 12, 2959-
679 2968, DOI 10.5194/acp-12-2959-2012, 2012.

680 Riedel, T. P., Wolfe, G. M., Danas, K. T., Gilman, J. B., Kuster, W. C., Bon, D. M., Vlasenko, A., Li, S. M., Williams,
681 E. J., Lerner, B. M., Veres, P. R., Roberts, J. M., Holloway, J. S., Lefer, B., Brown, S. S., and Thornton, J. A.:
682 An MCM modeling study of nitryl chloride (ClNO₂) impacts on oxidation, ozone production and nitrogen oxide
683 partitioning in polluted continental outflow, *Atmos Chem Phys*, 14, 3789-3800, 10.5194/acp-14-3789-2014,
684 2014.

685 Riemer, N., Vogel, H., Vogel, B., Anttila, T., Kiendler-Scharr, A., and Mentel, T. F.: Relative importance of organic
686 coatings for the heterogeneous hydrolysis of N₂O₅ during summer in Europe, *J Geophys Res-Atmos*, 114, 2009.

687 Roberts, J. M., Osthoff, H. D., Brown, S. S., Ravishankara, A. R., Coffman, D., Quinn, P., and Bates, T.: Laboratory
688 studies of products of N₂O₅ uptake on Cl⁻ containing substrates, *Geophys Res Lett*, 36, Artn L20808.
689 10.1029/2009gl040448, 2009.

690 Rollins, A. W., Kiendler-Scharr, A., Fry, J. L., Brauers, T., Brown, S. S., Dorn, H. P., Dube, W. P., Fuchs, H., Mensah,
691 A., Mentel, T. F., Rohrer, F., Tillmann, R., Wegener, R., Wooldridge, P. J., and Cohen, R. C.: Isoprene oxidation
692 by nitrate radical: alkyl nitrate and secondary organic aerosol yields, *Atmos Chem Phys*, 9, 6685-6703, 2009.

693 Sarwar, G., Simon, H., Xing, J., and Mathur, R.: Importance of tropospheric ClNO₂ chemistry across the Northern
694 Hemisphere, *Geophys Res Lett*, 41, 4050-4058, 10.1002/2014gl059962, 2014.

695 Spittler, M., Barnes, I., Bejan, I., Brockmann, K. J., Benter, T., and Wirtz, K.: Reactions of NO₃ radicals with
696 limonene and alpha-pinene: Product and SOA formation, *Atmos Environ*, 40, S116-S127,
697 10.1016/j.atmosenv.2005.09.093, 2006.

698 Stutz, J., Wong, K. W., Lawrence, L., Ziemba, L., Flynn, J. H., Rappengluck, B., and Lefer, B.: Nocturnal NO₃ radical
699 chemistry in Houston, TX, *Atmos Environ*, 44, 4099-4106, 10.1016/j.atmosenv.2009.03.004, 2010.

700 Su, X., Tie, X. X., Li, G. H., Cao, J. J., Huang, R. J., Feng, T., Long, X., and Xu, R. G.: Effect of hydrolysis of N₂O₅
701 on nitrate and ammonium formation in Beijing China: WRF-Chem model simulation, *Sci Total Environ*, 579,
702 221-229, 10.1016/j.scitotenv.2016.11.125, 2017.

703 Tan, Z., Fuchs, H., Lu, K., Hofzumahaus, A., Bohn, B., Broch, S., Dong, H., Gomm, S., Häsel, R., He, L., Holland,
704 F., Li, X., Liu, Y., Lu, S., Rohrer, F., Shao, M., Wang, B., Wang, M., Wu, Y., Zeng, L., Zhang, Y., Wahner, A.,
705 and Zhang, Y.: Radical chemistry at a rural site (Wangdu) in the North China Plain: observation and model
706 calculations of OH, HO₂ and RO₂ radicals, *Atmos. Chem. Phys.*, 17, 663-690, 10.5194/acp-17-663-2017, 2017.

707 Tang, M. J., Schuster, G., and Crowley, J. N.: Heterogeneous reaction of N₂O₅ with illite and Arizona test dust
708 particles, *Atmos Chem Phys*, 14, 245-254, 2014.

709 Tang, M. J., Thieser, J., Schuster, G., and Crowley, J. N.: Kinetics and mechanism of the heterogeneous reaction of
710 N₂O₅ with mineral dust particles, *Phys Chem Chem Phys*, 14, 8551-8561, 2012.

711 Tang, M. J., Huang, X., Lu, K. D., Ge, M. F., Li, Y. J., Cheng, P., Zhu, T., Ding, A. J., Zhang, Y. H., Gligorovski, S.,
712 Song, W., Ding, X., Bi, X. H., and Wang, X. M.: Heterogeneous reactions of mineral dust aerosol: implications
713 for tropospheric oxidation capacity, *Atmos Chem Phys*, 17, 11727-11777, 10.5194/acp-17-11727-2017, 2017.

714 Tham, Y. J., Wang, Z., Li, Q. Y., Yun, H., Wang, W. H., Wang, X. F., Xue, L. K., Lu, K. D., Ma, N., Bohn, B., Li, X.,
715 Kecorius, S., Gross, J., Shao, M., Wiedensohler, A., Zhang, Y. H., and Wang, T.: Significant concentrations of
716 nitryl chloride sustained in the morning: investigations of the causes and impacts on ozone production in a
717 polluted region of northern China, *Atmos Chem Phys*, 16, 14959-14977, 10.5194/acp-16-14959-2016, 2016.

718 Thornton, J. A., Braban, C. F., and Abbatt, J. P. D.: N₂O₅ hydrolysis on sub-micron organic aerosols: the effect of
719 relative humidity, particle phase, and particle size, *Phys Chem Chem Phys*, 5, 4593-4603, Doi
720 10.1039/B307498f, 2003.

721 Thornton, J. A., and Abbatt, J. P. D.: N₂O₅ reaction on submicron sea salt aerosol: Kinetics, products, and the effect
722 of surface active organics, *J Phys Chem A*, 109, 10004-10012, Doi 10.1021/Jp054183t, 2005.

723 Thornton, J. A., Kercher, J. P., Riedel, T. P., Wagner, N. L., Cozic, J., Holloway, J. S., Dube, W. P., Wolfe, G. M.,
724 Quinn, P. K., Middlebrook, A. M., Alexander, B., and Brown, S. S.: A large atomic chlorine source inferred from
725 mid-continental reactive nitrogen chemistry, *Nature*, 464, 271-274, Doi 10.1038/Nature08905, 2010.

726 Wagner, N. L., Riedel, T. P., Young, C. J., Bahreini, R., Brock, C. A., Dube, W. P., Kim, S., Middlebrook, A. M.,
727 Ozturk, F., Roberts, J. M., Russo, R., Sive, B., Swarthout, R., Thornton, J. A., VandenBoer, T. C., Zhou, Y., and
728 Brown, S. S.: N₂O₅ uptake coefficients and nocturnal NO₂ removal rates determined from ambient wintertime
729 measurements, *J Geophys Res-Atmos*, 118, 9331-9350, Doi 10.1002/Jgrd.50653, 2013.

730 Wahner, A., Mentel, T. F., and Sohn, M.: Gas-phase reaction of N₂O₅ with water vapor: Importance of heterogeneous
731 hydrolysis of N₂O₅ and surface desorption of HNO₃ in a large teflon chamber, *Geophys Res Lett*, 25, 2169-
732 2172, Doi 10.1029/98gl51596, 1998.

733 Wang, S. S., Shi, C. Z., Zhou, B., Zhao, H., Wang, Z. R., Yang, S. N., and Chen, L. M.: Observation of NO₃ radicals
734 over Shanghai, China, *Atmos Environ*, 70, 401-409, DOI 10.1016/j.atmosenv.2013.01.022, 2013.

735 Wang, M., Shao, M., Chen, W., Yuan, B., Lu, S., Zhang, Q., Zeng, L., and Wang, Q.: A temporally and spatially
736 resolved validation of emission inventories by measurements of ambient volatile organic compounds in Beijing,
737 China, *Atmos Chem Phys*, 14, 5871-5891, 10.5194/acp-14-5871-2014, 2014.

738 Wang, D., Hu, R. Z., Xie, P. H., Liu, J. G., Liu, W. Q., Qin, M., Ling, L. Y., Zeng, Y., Chen, H., Xing, X. B., Zhu, G.
739 L., Wu, J., Duan, J., Lu, X., and Shen, L. L.: Diode laser cavity ring-down spectroscopy for in situ measurement
740 of NO₃ radical in ambient air, *J Quant Spectrosc Ra*, 166, 23-29, 10.1016/j.jqsrt.2015.07.005, 2015.

741 Wang, H. C., and Lu, K. D.: Determination and Parameterization of the Heterogeneous Uptake Coefficient of
742 Dinitrogen Pentoxide (N₂O₅), *Prog Chem*, 28, 917-933, 10.7536/Pc151225, 2016.

743 Wang, T., Tham, Y. J., Xue, L. K., Li, Q. Y., Zha, Q. Z., Wang, Z., Poon, S. C. N., Dube, W. P., Blake, D. R., Louie,
744 P. K. K., Luk, C. W. Y., Tsui, W., and Brown, S. S.: Observations of nitryl chloride and modeling its source and
745 effect on ozone in the planetary boundary layer of southern China, *J Geophys Res-Atmos*, 121, 2476-2489,
746 10.1002/2015jd024556, 2016.

747 Wang, H. C., Chen, J., and Lu, K. D.: Development of a portable cavity-enhanced absorption spectrometer for the
748 measurement of ambient NO₃ and N₂O₅: experimental setup, lab characterizations, and field applications in a
749 polluted urban environment, *Atmos Meas Tech*, 10, 1465-1479, 10.5194/amt-10-1465-2017, 2017a.

750 Wang, H. C., Lu, K. D., Tan, Z. F., Sun, K., Li, X., Hu, M., Shao, M., Zeng, L. M., Zhu, T., and Zhang, Y. H.:
751 Model simulation of NO₃, N₂O₅ and ClNO₂ at a rural site in Beijing during CAREBeijing-2006, *Atmos Res*,
752 196, 97-107, 10.1016/j.atmosres.2017.06.013, 2017b.

753 Wang, H. C., Lu, K. D., Chen, X. R., Zhu, Q. D., Chen, Q., Guo, S., Jiang, M. Q., Li, X., Shang, D. J., Tan, Z. F:
754 High N₂O₅ concentrations observed in urban Beijing: Implications of a large nitrate formation pathway.,
755 *Environ. Sci. Technol. Lett.*, 10, doi: 10.1021/acs.estlett.7b00341, 2017c.

756 Wang, X. F., Wang, H., Xue, L. K., Wang, T., Wang, L. W., Gu, R. R., Wang, W. H., Tham, Y. J., Wang, Z., Yang, L.
757 X., Chen, J. M., and Wang, W. X.: Observations of N₂O₅ and ClNO₂ at a polluted urban surface site in North
758 China: High N₂O₅ uptake coefficients and low ClNO₂ product yields, *Atmos Environ*, 156, 125-134,
759 10.1016/j.atmosenv.2017.02.035, 2017.

760 Wang, Z., Wang, W. H., Tham, Y. J., Li, Q. Y., Wang, H., Wen, L., Wang, X. F., and Wang, T.: Fast heterogeneous
761 N₂O₅ uptake and ClNO₂ production in power plant and industrial plumes observed in the nocturnal residual
762 layer over the North China Plain, *Atmos Chem Phys*, 17, 12361-12378, 2017. 10.5194/acp-17-12361-2017

763 Wayne, R. P., Barnes, I., Biggs, P., Burrows, J. P., Canosamas, C. E., Hjorth, J., Lebras, G., Moortgat, G. K., Perner,
764 D., Poulet, G., Restelli, G., and Sidebottom, H.: The Nitrate Radical - Physics, Chemistry, and the Atmosphere,
765 *Atmos Environ a-Gen*, 25, 1-203, Doi 10.1016/0960-1686(91)90192-A, 1991.

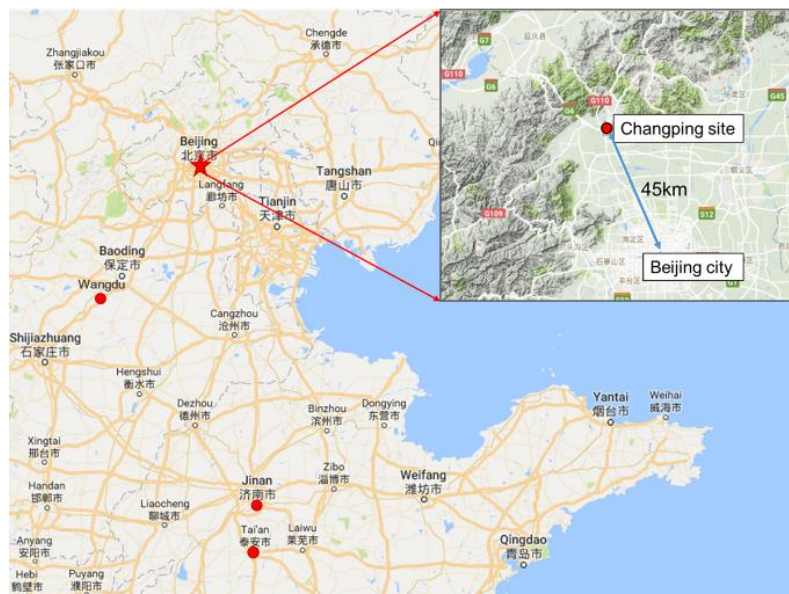
766 Xue, L. K., Saunders, S. M., Wang, T., Gao, R., Wang, X. F., Zhang, Q. Z., and Wang, W. X.: Development of a
767 chlorine chemistry module for the Master Chemical Mechanism, *Geosci Model Dev*, 8, 3151-3162,
768 10.5194/gmd-8-3151-2015, 2015.

769 Ye, N. N. L., K. D. Dong, H. B. Wu, Y. S. Zeng, L. M and Zhang, Y. H.: A study of the Water-Soluble Inorganic Salts
770 and Their Gases Precursors at Wangdu Site in the Summer Time, *Acta Scientiarum Naturalium Universitatis*,
771 52, p1109-1117, doi.org/10.13209/j.0479-8023.2016.116, 2016.

772 Yue, D. L., Hu, M., Wu, Z. J., Wang, Z. B., Guo, S., Wehner, B., Nowak, A., Achtert, P., Wiedensohler, A., Jung, J.,
773 Kim, Y. J., and Liu, S.: Characteristics of aerosol size distributions and new particle formation in the summer in
774 Beijing, *J Geophys Res-Atmos*, 114, Artn D00g1210.1029/2008jd010894, 2009.

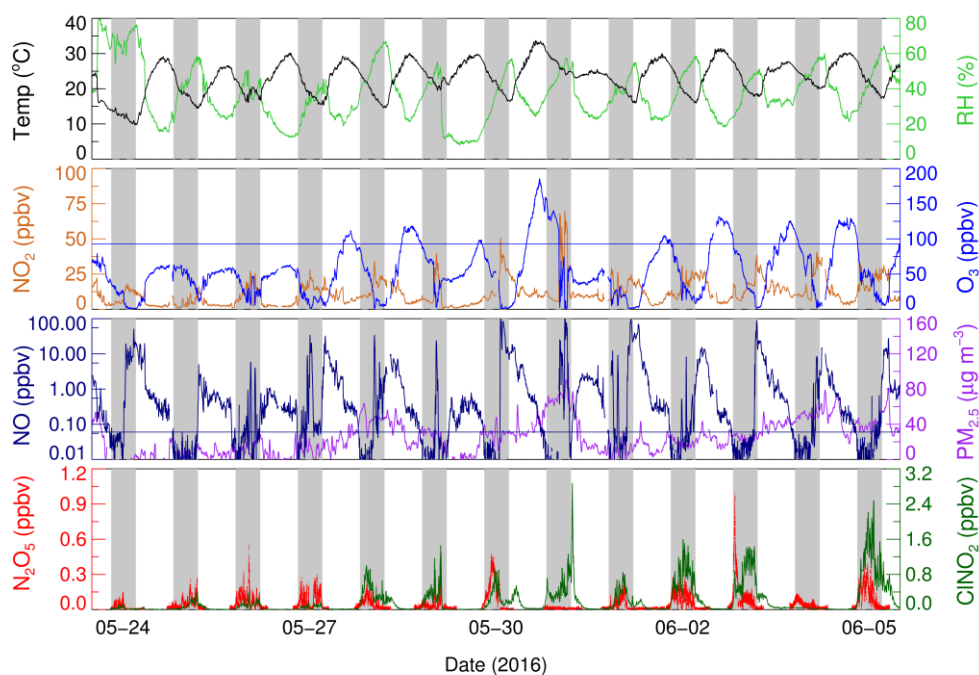
775 Zheng, J., Hu, M., Du, Z. F., Shang, D. J., Gong, Z. H., Qin, Y. H., Fang, J. Y., Gu, F. T., Li, M. R., Peng, J. F., Li, J.,
776 Zhang, Y. Q., Huang, X. F., He, L. Y., Wu, Y. S., and Guo, S.: Influence of biomass burning from South Asia at
777 a high-altitude mountain receptor site in China, *Atmos Chem Phys*, 17, 6853-6864, 10.5194/acp-17-6853-2017,
778 2017.

779



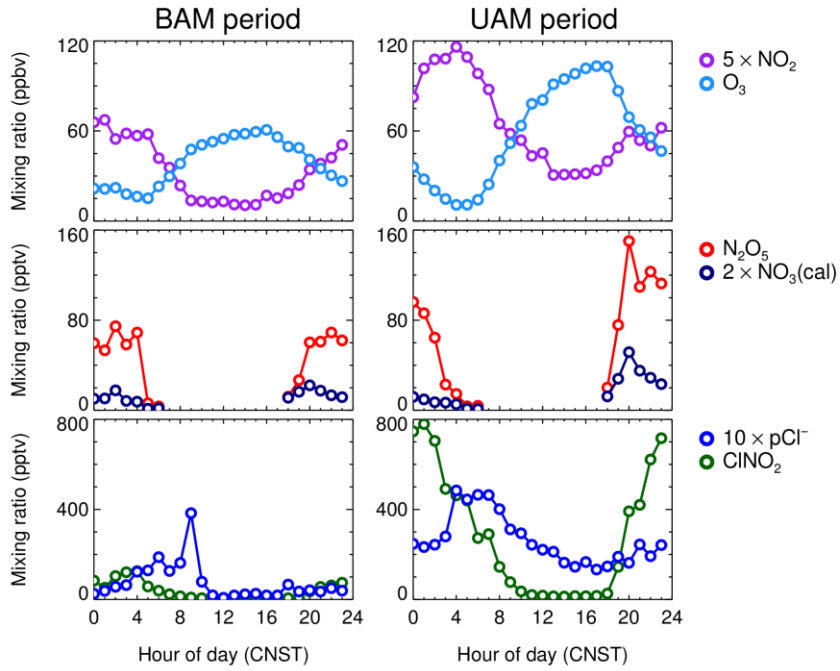
780

781 **Figure 1.** Map of Beijing and surrounding area. The red star shows the location of the Changping site,
 782 and red dots show other sites where previous N_2O_5 measurements were conducted in the North China
 783 Plain (NCP), including Wangdu, Jinan and Mt. Tai (Tai' an).



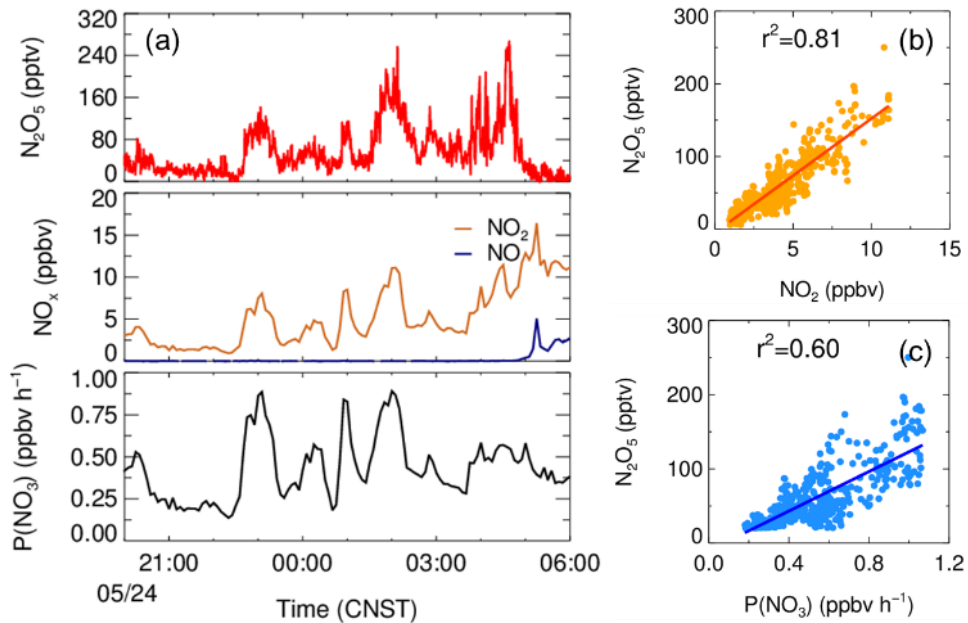
784

785 **Figure 2.** Time series of N_2O_5 , ClNO_2 and other relevant parameters. The blue line in the O_3 panel
 786 denotes Chinese national air quality standard for O_3 (ca. 93 ppbv for the surface conditions). The
 787 black line in the NO panel denotes 0.06 ppbv.



788

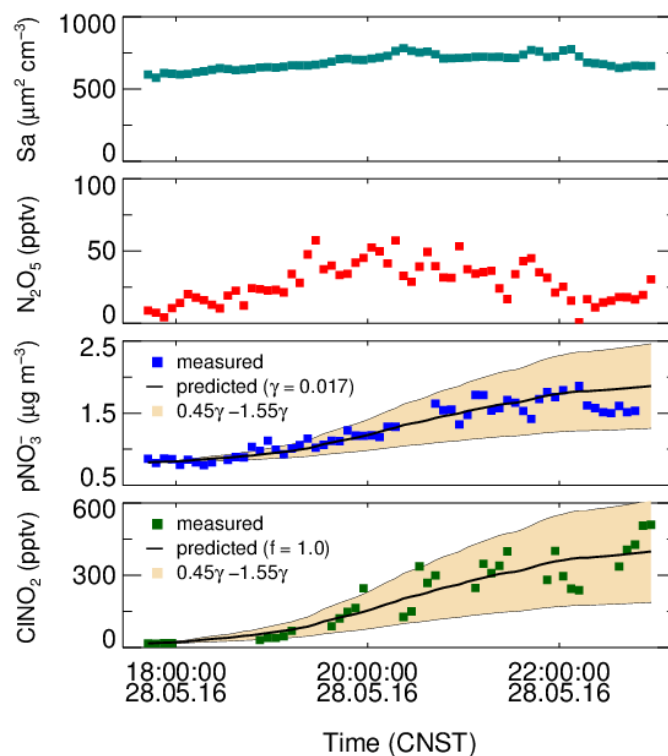
789 **Figure 3.** Mean diurnal profiles of $5 \times \text{NO}_2$, O_3 , N_2O_5 , $2 \times \text{NO}_3$ (calculated), ClNO_2 , and $10 \times \text{pCl}^-$. The
 790 left three panels depict the background air mass (BAM) period and the right three panels depict the
 791 urban air mass (UAM) period.



792

793 **Figure 4.** The correlation of the mixing ratio of N_2O_5 and NO_2 and the production rate of NO_3 on the
 794 night of May 24.

795

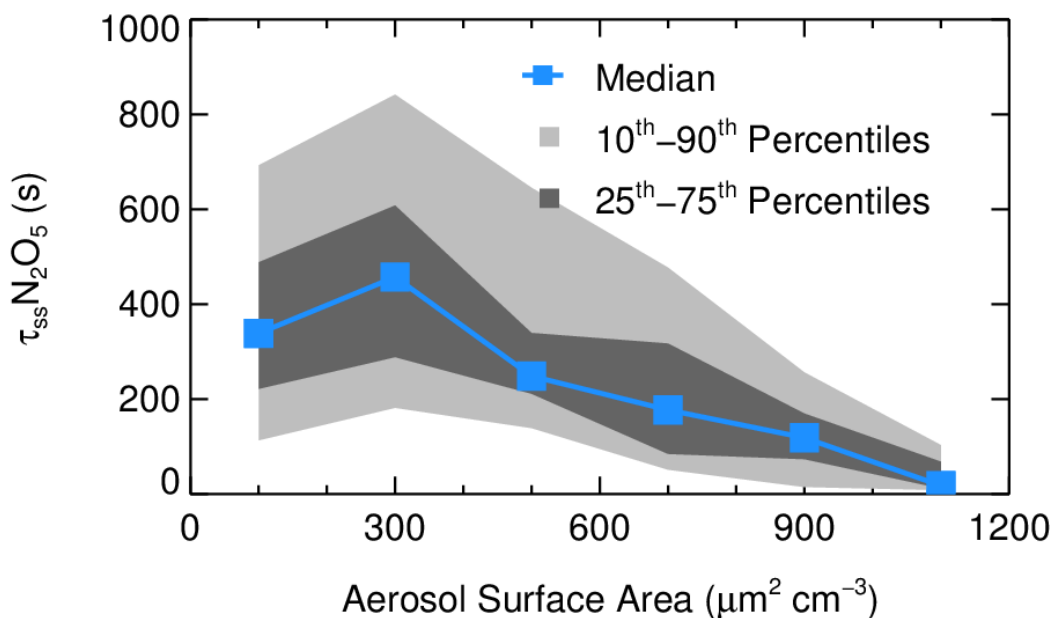


796

797 **Figure 5.** The best fit of γ and f to reproduce the observed ClNO_2 and pNO_3^- with an offset on May 28.

798 The black lines are the predicted results of the integrated NO_3^- and ClNO_2 by using the observed S_a

799 and N_2O_5 .

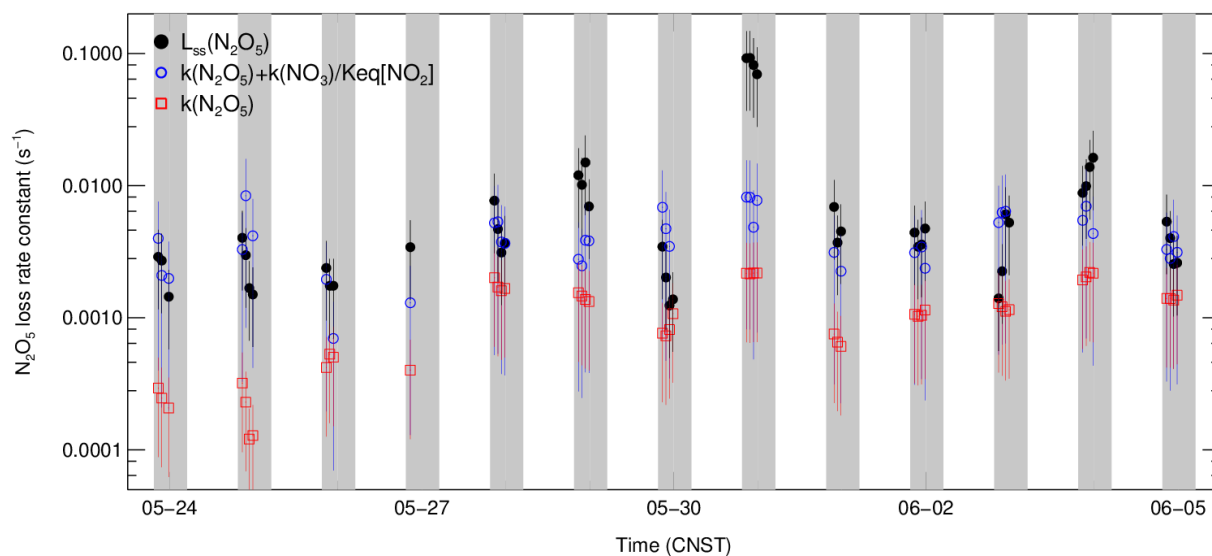


800

801 **Figure 6.** The dependence of N_2O_5 lifetime on aerosol surface area. Data were selected from 20:00 to

802 04:00 and are shown as medians, 25 - 75th percentile ranges, and 10 - 90th percentile ranges, as shown

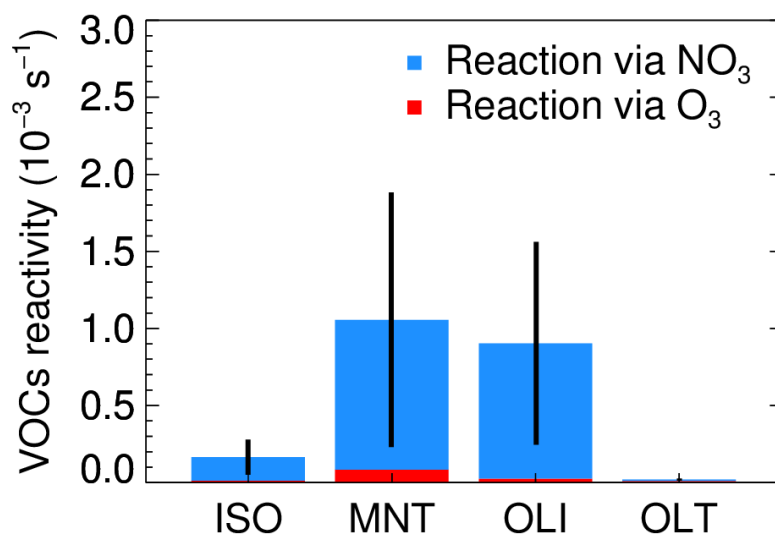
803 in the legend.



804

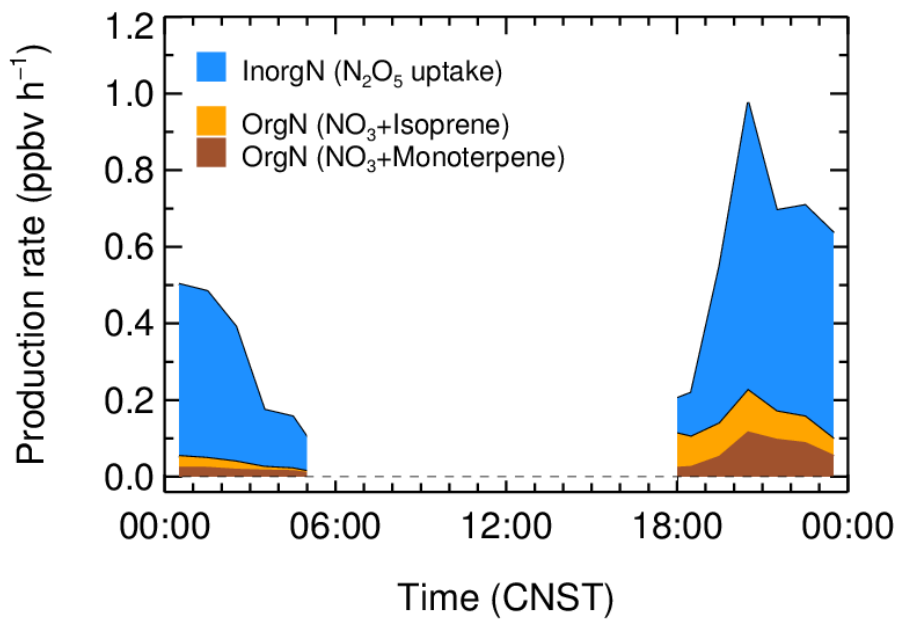
805 **Figure 7.** Time series of the individual N_2O_5 loss terms and the loss rate constant of N_2O_5 in steady
 806 state ($L_{ss}(N_2O_5)$).

807



808

809 **Figure 8.** The nighttime VOCs reactivity of NO_3 and O_3 (defined as the first order loss rate of VOCs
 810 ~~initialized~~ by oxidants, include NO_3 and O_3); the VOCs are classified as isoprene (ISO),
 811 monoterpene (MNT), the terminal alkenes (OLT) and the internal alkenes (OLI). The data were
 812 selected from 20:00 to the next day 04:00.



813

814 **Figure 9.** The nighttime production rate of organic and inorganic nitrates; the inorganic nitrates were
 815 calculated from the N₂O₅ heterogeneous hydrolysis, and the ON were calculated by the NO₃ reacted
 816 with isoprene and monoterpene.

817

818

819 **Table 1.** The observed gas and particle parameters used in this analysis during the campaign.

Species	Limit of detection	Methods	Accuracy
N ₂ O ₅	2.7 pptv (1 σ , 1 min)	CEAS	\pm 19%
ClNO ₂	16 pptv (2 σ , 1 min)	FIGAERO-ToF-CIMS	\pm 23%
NO	60 pptv (2 σ , 1 min)	Chemiluminescence	\pm 20%
NO ₂	0.3 ppbv (2 σ , 1 min)	Mo convert	\pm 50%
O ₃	0.5 ppbv (2 σ , 1 min)	UV photometry	\pm 5%
Aerosol surface area	- (4 min)	SMPS, APS	\pm 30%
VOCs	0.1 ppbv (5 min)	PTR-MS	\pm 30%
PM _{2.5}	0.1 $\mu\text{g m}^{-3}$ (1 min)	TEOM	\pm 5%
PM _{1.0} components	0.15 $\mu\text{g m}^{-3}$ (4 min)	HR-ToF-AMS	\pm 30%

820

821 **Table 2.** Summary of the field observed ambient ClNO₂/N₂O₅.

Location	Region	ClNO ₂ /N ₂ O ₅ ^a	References
Beijing, China	Inland	0.7 – 42.0 (5.4)	This work
Wangdu, China	Inland	0.4 - 131.3 (29.5)	Tham et al., 2016
Jinan, China	Marine	25.0 - 118.0 ^b	X. F. Wang et al., 2017
Mt. Tai, China	Marine	~ 4.0	Z. Wang et al., 2017
Hong Kong, China	Marine	0.1 - 2.0	T. Wang et al., 2016
London, UK	Inland	0.02 - 2.4 (0.51)	Bannan et al., 2015
Frankfurt, Germany	Inland	0.2 - 3.0	Phillips et al., 2012
Colorado, USA	Inland	0.2 - 3.0	Thornton et al., 2010
California, USA	Marine	~ 0.2 - 10.0 ^c	Mielke et al., 2013

822 Note: ^a Daily average results; ^b Power plant plume cases at Mt. Tai in Shandong, China; ^c Estimated according to Mielke
823 et al., (2013).

824

Table 3. Summary of the average $\gamma \times f$ values derived in the field observations.

Location	Region	$\gamma \times f$	References
Beijing, China	suburban	0.019 ± 0.009	This work
Frankfurt, Germany	suburban	0.014	Phillips et al., 2016
Mt. Tai, China	suburban	0.016	Z. Wang et al., 2017
Jinan, China	urban	<0.008	X. F. Wang et al., 2017
California, USA	urban	0.008	Mielke et al., 2013

825

826

Table 4. List of the N_2O_5 uptake coefficients and the yield of ClNO_2 in this campaign.

Start time	End time	γ	f
05/25 00:00	05/25 05:00	0.047 ± 0.023	0.60 ± 0.30
05/25 18:30	05/25 23:00	0.012 ± 0.006	1.0 ± 0.50
05/27 19:00	05/27 20:40	0.040 ± 0.032	0.50 ± 0.40
05/28 19:00	05/28 23:00	0.017 ± 0.009	1.0 ± 0.50
05/30 21:00	05/31 00:00	0.055 ± 0.030	0.55 ± 0.30

827